A MONTE CARLO METHOD TO ESTIMATE RADIATION DOSE FROM CONE BEAM COMPUTED TOMOGRAPHY

Jacob S. Dunn

A thesis submitted to the faculty at the University of North Carolina at Chapel Hill in partial fulfillment of the requirements for the degree of Master of Science in the School of Dentistry (Oral and Maxillofacial Radiology).

Chapel Hill
2015

Approved by:

John B. Ludlow

André Mol

Marija Ivanovic

ABSTRACT

Jacob S. Dunn: A Monte Carlo method to estimate radiation dose from cone beam computed tomography
(Under the direction of John B. Ludlow)

Objectives: This study compares effective dose determination of four large field of view CBCT units (NewTom-3G, Galileos Comfort Plus, CS-9300, iCat-FLX,) using a Monte Carlo software analysis method (PCXMC) and dosimetry using anthropomorphic phantoms.

Methods: Previous research provided phantom effective dose comparisons. Field-of-view and phantom positioning were duplicated in the software. Software and phantom dosimetry values were compared. Descriptive statistics, chi-square, and logistic regression, were used to analyze the data. The null-hypothesis that there is no statistically significant difference between the dosimetry values of the anthropomorphic phantom and the calculated values of the PCXMC software was tested.

Results: PCXMC simulated scans produced dose values within 20% of the phantom dosimetry 48-58% of the time.

Conclusions: While the software calculations are simpler to perform than phantom dosimetry, imprecise calculated results make this program less effective for CBCT dosimetry in dentistry.

ACKNOWLEDGEMENTS

I would like to express my sincere appreciation for my mentor and committee for their unyielding support, and particularly for their ability (and faith) to operate from 10,000 feet.

Supported in part by the National Institute of Dental and Craniofacial Research of the National Institutes of Health under award number R21DE022160. The content is solely the responsibility of the authors and does not necessarily represent the official views of the National Institutes of Health.

TABLE OF CONTENTS

LIST OF TABLES

LIST OF FIGURES

LIST OF ABBREVIATIONS AND SYMBOLS

BREP	Boundary representation (phantom)
CBCT	Cone beam computed tomography
DAP	Dose area product
ENIAC	Electronic Numerical Integrator and Computer
FOV	Field of View
ICRP	International Commission on Radiological Protection
LANL	Los Alamos National Laboratory
MC	Monte Carlo
MDCT	Multi-detector computed tomography
MIRD	Medical Internal Radiation Dose
MOSFET	Metal-oxide-semiconductor field-effect transistor
MR	Magnetic Resonance
NCRP	National Council on Radiation Protection and Measurements
ORNL	Oak Ridge National Laboratory
OSLD	Optically stimulated luminescent dosimeter
RANDO	Radiation analog dosimetry system
SID	Source to image distance
SMV	Submentovertex
TLD	Thermoluminescent dosimeter
TMJ	Temporomandibular joint
VCH	Visible Chinese Human
Π	The numerical value of the ratio of the circumference of a circle to its diameter. NOT made of cherry. Although a whole pie CAN be used to calculate π. Read on to find out!
μ	Micro-, a unit denoting a factor of 10^{-6}

DEVELOPMENT OF MONTE CARLO

> "The first thoughts and attempts I made to practice [the Monte Carlo method] were suggested by a question which occurred to me in 1946 as I was convalescing from an illness and playing solitaires. The question was what are the chances that a Canfield solitaire laid out with 52 cards will come out successfully? After spending a lot of time trying to estimate them by pure combinatorial calculations, I wondered whether a more practical method than "abstract thinking" might not be to lay it out say one hundred times and simply observe and count the number of successful plays. This was already possible to envisage with the beginning of the new era of fast computers, and I immediately thought of problems of neutron diffusion and other questions of mathematical physics, and more generally how to change processes described by certain differential equations into an equivalent form interpretable as a succession of random operations."[1]

These remarks were made by Stanislaw Marcin Ulam, a Polish-American scientist who was one of the primary contributors in the development of the Monte Carlo method. Born in 1909 Lviv, in a Polish area of now Ukraine that was then part of the Austro-Hungarian Empire, Ulam studied mathematics throughout Europe until he was invited in 1935 to come to the Institute for Advanced Study in Princeton, New Jersey.[2] This led to opportunities for research at Harvard University in Cambridge, Massachusetts, until he became an assistant professor at the University of Wisconsin-Madison.[2]

In 1943, he was invited to join a special project near Santa Fe, New Mexico. This top secret group was located at the Los Alamos National Laboratory, which research today is well known as the Manhattan Project. His work ultimately led him to consider multiplicative systems and the statistics of branching. These are situations in which particles interact with a system – with particulate type, number, position, momentum, and other intrinsic properties potentially changing with time.[3] The branches – or individual steps of the process, utilized probability functions to determine the properties of the next generation of particles within the system.[3] A group of other researchers, including Nicholas Metropolis and John von Neumann,

had been working out calculations on the first general electronic computer, called the Electronic Numerical Integrator and Computer (ENIAC).[4] While Ulam was reviewing these calculations, he realized that the faster calculating ability of this machine would allow the reality of a method of statistical analysis he had considered while playing solitaire during a previous convalescence.[1] Von Neumann applied Ulam's thought to a proposal to evaluate the behavior of neutrons during nuclear fission.[5] Metropolis code named it "The Monte Carlo method" because Ulam had mentioned an uncle who frequented the Monte Carlo casinos.[4] Together, they published an early, unclassified paper on the subject.[6]

The Monte Carlo Method

The Monte Carlo (MC) method is a statistical approach to solving problems in systems in which there is a degree of uncertainty. There are many methods to accomplish the task, but basic points include the following: the definition of the domain of possible inputs, the generation of random inputs based on probability actions within that domain, the computation of results (calculating a successful 'hit' or not, based on the definition of the domain), and finally an aggregation of the results.[7] A simple example of this would be an attempt to calculate the value of π. If a circle is circumscribed within a square and drawn on the floor, the ratio of the areas (circle to square) is $\pi/4$. If many, many pins were dropped at random within the entirety of the square, and counted at the end, the number of points within the circle relative to the entirety of the square would also be very close to the fraction, $\pi/4$.[7] This is one basic example of using the Monte Carlo method, including the inherent random sampling, to solve a mathematical problem.

This method is particularly suited to the evaluation of radiation transport in systems.[8] The simulation is performed by creating and following life histories of many photons. Variables required for the photon evaluation include the photon position, the direction, the energy, and time. Variables required for the interaction medium include geometry of the medium, location

of internal structures (organs) and characteristics of the organs (volume, shape, and attenuation). The distribution of the photons utilize both measurements and theoretical properties of x-rays.[7] Kalos and Whitlock effectively describe the steps involved:

> 1. Pick a set of source variables (initial state of system).
> 2. Follow the x-ray until it interacts with an atom.
> 3. Determine whether the x-ray scatters
> -if so, repeat from step 2;
> -if not, terminate the history.
> Steps 2 and 3 are repeated until the x-ray photon is absorbed or is no longer capable of effecting the answer to any appreciable extent.
> 4. Repeat the whole process from step 1 as many times as necessary to achieve the accuracy needed for the solution.
> 5. Take arithmetic average of answers of all the histories.[7]

This sequence describing radiation transport in a system is essentially a "random walk" or a Markov chain, a process that has stepwise transitions involving randomness and probability.[9, 10] Each step is a collision event, which outcome depends on the characteristics of the radiation and interaction medium. Modeling of these collisions requires listing the possible events, then assigning the probability of each of those events occurring. Just like with Hollywood actors, the life history of the photon is closely followed until interest in it is lost or it is terminated.[7] Interest is lost when the photon is too low in energy to affect the answer, and termination occurs with a photoelectric effect or when it exits the system. To summarize, the process simulates an x-ray photon with "random position, direction, and time, which travels in straight-line segments whose lengths are random; the photon interacts with the atoms constituting the medium at random, and its life history is concluded at random."[7]

THE USE OF MONTE CARLO WITH DENTAL CBCT: REVIEW OF LITERATURE

A search for the term 'monte carlo' on PubMed yields nearly 40,000 results, illustrating the near ubiquity of this technique within medical physics, physical sciences, engineering, computer science, applied statistics, mathematics, artificial intelligence, image processing, biology, and even finance and business.[11, 12]

A review of the literature was completed on PubMed with the assistance of the School of Dentistry librarian. The search used the terms "cone beam computed tomography AND dosimetry AND 'monte carlo'", and "cone beam computed tomography AND dosimetry AND 'monte carlo' AND (dentistry OR dental)", and "'monte carlo' AND (dentistry OR dental)".

The majority of the articles involving cone beam computed tomography (CBCT) and Monte Carlo (MC) programs evaluate dose characteristics of the onboard CBCT as part of a linear accelerator used in image guided radiation therapy (IGRT).[13-43] Additionally, dose evaluations of the associated electronic portal imaging devices are also common.[16, 21, 44-46] Other studies involve dose evaluation of multi-detector computed tomography (MDCT),[47-57] mega voltage CT,[58-61] medical CBCT involving neurology,[62] fluoroscopy,[63] angiography,[64] mammography,[65-67] and evaluation of internal radionuclides.[68, 69] Of image quality interest are articles that evaluate CBCT scatter with the goal of image quality improvement through scatter reduction.[70-72]

Monte Carlo Programs in Dentistry

A number of articles involving MC programs and dentistry pertain to the effect of dental restorations on doses within radiotherapy.[73-77] Other articles evaluate the effect on absorbed

dose when adding rare earth filters,[78] the electron paramagnetic resonance as a measure of dose within enamel,[79] enamel beam hardening in micro CT,[80] variations in light-induced fluorescence in enamel in the presence of caries,[81] maxillofacial fluoroscopy[82], and even estimates of caries in extended populations in Australia[83].

Several studies use Monte Carlo methods to evaluate dose with dental plain film radiography. Aps and co-workers investigated lateral radiographs and bitewing radiographs.[84] Batista and co-workers looked at the dose in panoramic images from conventional and CBCT machines.[85] Lee and co-workers (2012) studied the effect of collimation in cephalography.[86] Nicopoulou-Karayianni and co-workers looked at radiation absorbed doses at titanium-bone interfaces in diagnostic dental radiography.[87] Walker and co-workers proposed diagnostic references levels for intraoral and panoramic radiography.[88]

Dr. Julian Gibbs led several studies at Vanderbilt University involving Monte Carlo analysis and dental radiography.[89-93] In 1982, Gibbs created a MC method to evaluate the dose distribution of an 80 kVp x-ray beam on a homogenous water phantom. He found no significant differences between the estimated doses and the doses measured with an ionization chamber. In 1984, he used the same MC program to evaluate dose from molar interproximal radiographs on a voxel CT phantom of an adult female cadaver. The voxels within the phantom were coded as air, lung, fat, muscle bone, or tooth, with attenuation factors coinciding with the then contemporary ICRP Reference Man recommendations. X-rays were programmed to operate at 90 kVp. The sequence was run with a target-skin distance of 20 cm with round collimation, and 40 cm with rectangular collimation. Gibbs found that the use of long-cone technique with rectangular collimation would reduce the cancer risk by a factor of 2.9.[90]

In 1987, Gibbs and co-workers used the same MC program and same female cadaver phantom to evaluate the dose to sensitive organs during intraoral radiography. The investigators found that organ doses generally increase with increasing beam energy. Largest doses were found in organs near the primary beam. In 1989, using the same MC program and

female cadaver phantom, Gibbs and co-workers simulated three radiographic examinations: chest, dental full mouth series, and dental panoramic. The investigators found that collimated dental examinations, while being less homogenous than the chest examination, concentrated dose to organs of the head and neck.[92]

In 2000, Gibbs used the same MC program and cadaver phantom to evaluate additional radiographic protocols, including submentovertex (SMV), temporomandibular joint (TMJ), cephalometric, and a chest PA and lateral images. Organ doses for each projection were determined at 70, 80, and 90 kVp. Gibbs found that effective dose and effective dose equivalent calculations varied significantly between organs, depending on image protocol.[93]

Monte Carlo Programs and Dental CBCT

Fully six articles deal with dosimetry using Monte Carlo methods on dental CBCT.[94-99] In 2010, Vassileva and co-workers used PCXMC (STUK, Helsinki, Finland) to estimate effective dose of the ILUMA Ultra CBCT (IMTEC Imaging, Ardmore, OK). Software estimated effective doses were lower than those calculated with RANDO (The Phantom Laboratory, Salem, NY) phantom dosimetry by Ludlow and Ivanovic by over 68% with ICRP 103 recommendations.[97, 100]

In 2011, Zhang and co-workers evaluated the 3D Accuitomo 170 unit (J Morita, Japan), using the BEAMnrc/EGSnrc MC code system to simulate x-ray generation, filtration, and collimation. Kerma free-in-air at the isocenter was validated by comparison against measured air kerma in water in a cylindrical water phantom. Discrepancies between the two measurements varied less than 15%.[98] In 2013, Zhang and co-workers investigated the 3D Accuitomo 170 and the Scanora 3D (Soredex, Finland). The BEAMnrc/EGSnrc MC code was used again, on four phantoms: the two International Commission on Radiological Protection (ICRP) reference voxel phantoms (AM and AF), the Zubal phantom, which is another CT voxel phantom, and the VCH (Visible Chinese Human) phantom, which is based on axial photographs sections of a Chinese cadaver. For the Accuitomo, FOVs included a 17x12 cm, 10x10 cm, and 6x6

cm. For the Scanora, a 14.5x7.5 cm, 10x7.5 cm, and 6x6 cm FOV was included. Absorbed organ dose and effective dose were calculated. Of note is the fact that the thyroid was not part of the head/neck of any of the four phantoms, and as such, it was not included in the calculation of effective dose.[99] The authors found that organ dose varied as much as 112% between phantoms, and that between the two machines examined, variation of organ doses between phantoms was greater than dose differences between machines. Effective dose varied up to 30% (in terms of coefficient of variation, defined as the ratio of standard deviation to the mean, expressed as a percentage). Differences in phantom anatomy were was surmised as the reasoning behind the difference in effective dose.

In 2012, Koivisto and co-workers evaluated effective dose on the Promax 3D CBCT (Planmeca, Helsinki, Finland) using new metal-oxide semiconductor field-effect transistors (MOSFET) dosimeter devices, and compared them with PCXMC estimated results. The dosimeters were placed in a RANDO phantom according to protocol described by Ludlow and co-workers.[101] The field of view (FOV) was 8x8cm, and positioned to capture the oral cavity volume. The phantom scans and simulations were performed at various heights on the z-axis, to evaluate vertical positioning on effective dose. Both the phantom and the simulation noted a distinct relationship between the presence of the thyroid within the scan, (and accordingly that organ's equivalent dose) and total effective dose. The difference between MOSFET measured and PCXMC estimated effective dose differed by as much as 52%, and differences in individual organ equivalent doses varied as much as 600%.[102] Differences between the two were equated to differences in the mathematically modeled and physical phantom, regarding shape, volume, and positioning of the organs, particularly the thyroid. Additionally, the authors noted that small differences in phantom head position had a substantial effect on effective dose.[102]

In 2012, Morant and co-workers evaluated the dose on an iCat next-generation CBCT (Imaging Sciences International, Hatfield, PA) using MC program Electron Gamma Shower V4 (EGS4) (Stanford University, Palo Alto, CA) and compared the estimated results with ionization

chamber measurements and thermoluminescent dosimeters (TLD) in a water-filled Remab male adult phantom (Alderson Research Laboratory). The imaging protocols examined were the "Landscape 13cm" and "Extended Field of View (Cephalometric, E-FOV)". Within the ionization chambers, percent difference between the two methods ranged up to 6%. Within the phantom, relative differences between the organ dose values (mGy to air) ranged 1-84%, although more than half had less than 13% difference. Statistical uncertainties of the MC program ranged 7-19% for dose values ≥1 mGy, and increased to 100-130% for values of 0.01 mGy.[95]

Morant and co-workers again in 2013 studied MC program EGS4 simulated doses on the iCat next-generation CBCT. The ICRP voxel adult male and female reference phantoms (AM and AF) were evaluated. Nine different FOVs were simulated. The authors found that organ and effective dose varied according to FOV, beam acquisition angles and positioning. The full head scan (23 x 17cm FOV) estimated effective dose was 47% less than the results of Ludlow and Ivanovic, however, Davies and co-workers showed reasonable agreement with the other imaging protocols.[100, 103]

PCXMC Studies in the Literature

A review of the literature was completed on PubMed with the search term "PCXMC." Aside from the studies mentioned previously, the majority of studies involved radiography within the pediatric community.[104-126] Other studies included fluoroscopy,[127-133] angiography,[134, 135] other interventional radiography,[136-139] tomosynthesis,[140-143] and CBCT as a part of image guided radiation therapy.[144-146] On the more technical side, studies investigated dose relating to structural shielding,[147] source-to-image distance (SID),[148, 149] dose-area-product (DAP),[150] collimation,[151] different x-ray spectra,[152] and projection angles.[153, 154]

BACKGROUND

Shortly after the initial discovery of x-rays by Wilhelm Roentgen, dentistry began incorporating radiology as a means of diagnosis.[155] Through the years, the technology and use has kept pace with the increasing range and variation of treatment. The utilization of radiology in dentistry was expanded with the development of commercial panoramic tomography in the early 1960s.[156] The parallel development of cone beam computed tomography (CBCT), although nearly thirty years later, also allowed new avenues and diagnostic abilities.[157]

The use of CBCT imaging has significantly increased within general dentistry, endodontics, oral surgery, periodontics, and orthodontics.[158-165] This increasing popularity of this technology is understandable with the ability of CBCT to reconstruct volumes, as well as present multi-planar simultaneous views, enabling the dental practitioner potentially much more information than previous two-dimensional radiography. Responding to the demand within the field, there are currently many firms that manufacture CBCT machines, with multiple models often produced within each company.[166]

CBCT is both similar to and different from medical computed tomography (CT). While they both use x-radiation in target exposure to achieve diagnostic information, the geometry of the beam, exposure parameters, and other aspects between the two systems are different.[167] Concordantly in medicine, the use of CT has significantly increased over the last 20 years.[168] The National Council on Radiation Protection and Measurements (NCRP) has stated that Americans were exposed to more than seven times as much ionizing radiation from diagnostic medical procedures in 2006 than they were in the early 1980s.[169, 170] Much of this is directly attributable to the nearly ubiquitous use of CT in diagnostic medical exams.[168] While the

radiation exposure from CBCT is usually lower than from CT, it is important to understand that risks of exposure still exist and that imaging principle of exposure parameters as low as reasonably achievable (ALARA) still applies to CBCT examination protocols.[171, 172]

With ionizing radiation, concern exists with both deterministic effects of radiation, those effects produced above a certain threshold dose, and stochastic effects, those effects that are random and probabilistic.[168, 173] With CBCT dose levels, the primary concern is with stochastic effects. Since limited data exists on radiation exposure and sequelae with small doses, extrapolation is required from higher dose evaluation.[168] A fundamental problem is that different CBCT units have different doses for similar exam protocols, and there is no standardization of dose for a specific image.[165] Accurate machine specific dosimetry is vital.

The current standard for dosimetry incorporates anthropomorphic phantoms, those commonly used include the radiation analog dosimetry system (RANDO) phantom (The Phantom Laboratory, Salem, NY), ATOM phantom (CIRS, Norfolk, VA), as well as a several others.[165, 174-185] This standard is time-consuming, costly, and technique sensitive.[186] A simple, inexpensive, and accurate method needs to be developed to measure dose and assess risk for a given scan.

The parallel quest in medicine to develop effective and inexpensive dosimetry has led to mathematical software analysis. One such software analysis method, named Monte Carlo, has become prevalent. The development actually began with the research in the 1940s on radiation shielding for the Manhattan Project.[12] Although the specific physical parameters of the project were known, the solutions were eluding the researchers using traditional mathematical methods. This is a broad heuristic approach, similar to the process of gambling many, many times (with a name like Monte Carlo, would you expect otherwise?) and recording your results, successful or not. The basic premise is that these simulations sample probability distribution for each variable to produce thousands of possible outcomes.[187] Monte Carlo simulations have become one of the most popular methods for modeling imaging systems, as well as being used

extensively for radiation dose estimation.[188, 189] Since there are many different Monte Carlo codes, the task is to evaluate individual programs for successful and accurate analysis.[12-14, 190, 191]

OBJECTIVES

This study compared effective dose determination of four large field of view CBCT units (CS-9300, NewTom-3G, iCat-FLX, and Galileos Comfort Plus) using a specific Monte Carlo software analysis method, PCXMC 2.0 (STUK, Helsinki, Finland), developed by Tapiovaara and co-workers for the Finnish Radiation Nuclear Safety Authority and dosimetry using anthropomorphic phantoms. The program uses a mathematically determined computational phantom. That information was used with the 2007 Tissue Weight factors from the ICRP to calculate the effective dose.

As accurate dosimetry is an important step in minimizing patient risk during radiologic examinations, accurate methods are needed to assess that risk. Within medicine, dosimetry has advanced significantly, and Monte Carlo methods are widely used. The goal of this study is to extend verification of Monte Carlo methods to additional dental CBCT units, and compare the accuracy of this specific software analysis methodology with dental dosimetry using anthropomorphic phantoms.

MATERIALS AND METHODS

This study compares simulated effective dose results from PCXMC, a user friendly, commercially available Monte Carlo method software application, with the effective dose results from previous research using dosimeters placed in tissue equivalent anthropomorphic phantoms. The previous research was completed by Ludlow and co-workers evaluating the NewTom 3G (Cefla Dental Group, Imola, IT) using a RANDO phantom and thermoluminescent dosimeters (TLDs), and the Galileos Comfort Plus HD (Sirona Dental Systems, Inc. Long Island City, NY), the CS 9300 (Carestream Dental, Atlanta, USA) and the iCat FLX (Imaging Sciences International, Hatfield, PA) using ATOM phantoms and optically stimulated dosimeters (OSLDs).[100, 101, 165, 192] Differences between the use of OSLs and TLDs, and the use of ATOM and RANDO phantoms were found to be less than 2% in the calculations of effective dose with ICRP 103 values.[192] Table 1Table *4* show the imaging protocols that were used on the physical phantoms for each machine. These protocols were duplicated in the PCXMC software, using the input parameters listed in table 5.

Table 1: NewTom 3G Included Image Protocol

FOV (width x height, cm)	Phantom (RANDO)	mAs	DAP (mGy cm2)
Full 30 x 30	Adult	8.1	362.2

Table 2: Galileos Comfort Plus Included Image Protocols

FOV (width x height, cm)	Collimation Setting	Patient Setting	HD Protocol	Phantom (ATOM)	mAs	DAP (mGy cm2)
Full 15 x 15	Full	child	On	Child	15	697
Full 15 x 15	Full	teen	On	Child, Adult	20	915
Full 15 x 15	Full	small adult	On	Child, Adult	25	1110
Full 15 x 15	Full	child	Off	Child	6	252
Full 15 x 15	Full	teen	Off	Child, Adult	8	328
Full 15 x 15	Full	small adult	Off	Child, Adult	10	387
Maxilla 15 x 7.5	Maxilla	child	On	Child	15	537
Maxilla 15 x 7.5	Maxilla	teen	On	Child, Adult	20	780
Maxilla 15 x 7.5	Maxilla	small adult	On	Child, Adult	25	958
Maxilla 15 x 7.5	Maxilla	child	Off	Child	6	194
Maxilla 15 x 7.5	Maxilla	teen	Off	Child, Adult	8	252
Maxilla 15 x 7.5	Maxilla	small adult	Off	Child, Adult	10	298
Mandible 15 x 7.5	Mandible	child	On	Child	15	391
Mandible 15 x 7.5	Mandible	teen	On	Child, Adult	20	513
Mandible 15 x 7.5	Mandible	small adult	On	Child, Adult	25	622
Mandible 15 x 7.5	Mandible	child	Off	Child	6	142
Mandible 15 x 7.5	Mandible	teen	Off	Child, Adult	8	184
Mandible 15 x 7.5	Mandible	small adult	Off	Child, Adult	10	217
Full 15 x 15	Full	large adult	On	Adult	30	1301
Full 15 x 15	Full	large adult	Off	Adult	12	470
Maxilla 15 x 7.5	Maxilla	large adult	On	Adult	30	1301
Maxilla 15 x 7.5	Maxilla	large adult	Off	Adult	12	362
Mandible 15 x 7.5	Mandible	large adult	On	Adult	30	729
Mandible 15 x 7.5	Mandible	large adult	Off	Adult	12	263

Table 3: CS9300 Included Image Protocols

FOV (width x height, cm)	Setting	Patient Setting	Protocol	Phantom (ATOM)	mAs	DAP (mGy cm2)
8 x 8	Jaws	Adult		Adult	50	716
10 x 5	Jaws Maxilla	Adult		Adult	39	471
10 x 5	Jaws Mandible	Adult		Adult	39	471
17 x 13.5	Craniofacial	Adult		Adult	45	1585
17 x 11	Sinus	Adult		Adult	65	2275
17 x 11	Craniofacial	Adult	Fast	Adult	26	898
10 x 10	Jaws	Adult		Adult	25	527
5 x 5 Right Posterior Maxilla	Dento-alveolar	Adult	Fast	Adult	60	366
5 x 5 Left Mid Maxilla	Dento-alveolar	Adult	Fast	Adult	60	366
5 x 5 Anterior Maxilla	Dento-alveolar	Adult	Fast	Adult	60	366
5 x 5 Left Posterior Mandible	Dento-alveolar	Adult	Fast	Adult	60	366
5 x 5 Right Mid Mandible	Dento-alveolar	Adult	Fast	Adult	60	366
5 x 5 Anterior Mandible	Dento-alveolar	Adult	Fast	Adult	60	366
5 x 5 Left	Auricular	Adult	Fast	Adult	120	873
8 x 8 Right	Auricular	Adult		Adult	76	1078
8 x 8 TMJ Left	TMJ	Adult		Adult	50	716
8 x 8	Jaws	Adolescent		Child	32	392
10 x 5	Jaws Maxilla	Adolescent		Child	25	258
10 x 5	Jaws Mandible	Adolescent		Child	25	258
17 x 13.5	Craniofacial	Adolescent		Child	45	1359
17 x 11	Craniofacial	Adolescent	Fast	Child	65	1950
10 x 10	Jaws	Adolescent		Child	26	770
5 x 5 Right Posterior Maxilla	Dento-alveolar	Adolescent	Fast	Child	25	454
5 x 5 Left Mid Maxilla	Dento-alveolar	Adolescent	Fast	Child	60	322
5 x 5 Anterior Maxilla	Dento-alveolar	Adolescent	Fast	Child	60	322
5 x 5 Left Posterior Mandible	Dento-alveolar	Adolescent	Fast	Child	60	322
5 x 5 Right Mid Mandible	Dento-alveolar	Adolescent	Fast	Child	60	322
5 x 5 Anterior Mandible	Dento-alveolar	Adolescent	Fast	Child	60	322
5 x 5 Left	Auricular	Adolescent	Fast	Child	120	755
8 x 8 Right	Auricular	Adolescent		Child	76	930
8 x 8 TMJ Left	TMJ	Adolescent		Child	32	392

Table 4: iCat FLX Included Image Protocols

FOV (width x height, cm)	Setting	Protocol	Phantom (ATOM)	mAs	DAP (mGy cm2)
8 x 8	Dental	QuickScan +	Adult, Child	6	40
16 x 6	Maxilla	QuickScan +	Adult, Child	6	49.6
16 x 6	Mandible	QuickScan +	Adult, Child	6	49.6
16 x 8	Both arches	QuickScan +	Adult, Child	6	64.9
16 x 11	Arches + TMJ	QuickScan +	Adult, Child	6	86.5
16 x 13	Standard Ceph	QuickScan +	Adult, Child	6	99.2
16 x 6	Maxilla	QuickScan	Adult, Child	10	168.5
8 x 8	Dental	QuickScan	Adult, Child	10	134.8
16 x 13	Standard Ceph	QuickScan	Adult, Child	10	349.4
16 x 8	Both arches	QuickScan	Adult, Child	10	219.6
16 x 11	Arches + TMJ	QuickScan	Adult, Child	10	301
16 x 6	Mandible	QuickScan	Adult, Child	10	163.6
8 x 8	Dental	Standard	Adult, Child	19	239
16 x 6	Maxilla	Standard	Adult, Child	19	302.9
16 x 6	Mandible	Standard	Adult, Child	19	291.4
16 x 8	Both arches	Standard	Adult, Child	19	388.9
16 x 11	Arches + Tmj	Standard	Adult, Child	19	543
16 x 13	Standard Ceph	Standard	Adult, Child	19	623.9
8 x 8	Dental	High Resolution	Adult	37	500.8
16 x 6	Maxilla	High Resolution	Adult	37	605.2
16 x 6	Mandible	High Resolution	Adult	37	611.6
16 x 8	Both arches	High Resolution	Adult	37	797.4
16 x 11	Arches + TMJ	High Resolution	Adult	37	1046
16 x 13	Standard Ceph	High Resolution	Adult	37	1257
23 x 17	EFOV	Standard	Adult	19	458.6
23 x 17	EFOV	Enhanced	Adult	37	877.6

Table 5: PCXMC Input Parameters

Projection	Projection angle relative to patient
Patient height	cm
Patient weight	kg
Patient age	years
X-ray tube voltage	kV
Machine Filtration	mm Al
Additional filter	mm Cu
FRD	Source to reference axis distance
X-ray beam width	cm, at FRD
X-ray beam height	cm, at FRD
Xref	FOV location coordinate, X-axis
Yref	FOV location coordinate, Y-axis
Zref	FOV location coordinate, Z-axis
Input dose quantity	EAK,EE,DAP,EAP or MAS
Input dose value	Dose value per image pulse

EAK – Air kerma, EE – Exposure, DAP – Dose Area Product
EAP – Exposure Area Product, MAS – Current-Time Product

PCXMC uses a computational phantom with anatomical data based on the mathematical hermaphrodite phantoms of Cristy and Eckerman.[193-195] These phantoms describe patients of various ages: a new-born, 1 year-old, 5 year-old, 10 year-old, 15 year-old, and adult. The tissues simulated in PCXMC are soft tissue (1.04 g/cm^3), lung tissue (0.296 g/cm^3), and skeleton (1.40 g/cm^3, newborn 1.22 g/cm^3).[193] Some changes have been made to the phantoms and internal organs to coincide with ICRP 103 tissue weighting factors.[193] Examples of these changes include additions of the mouth mucosa, salivary gland, extrathoracic airways, and prostate, modelled with guidance from ICRP Publication 89 as well as other studies.[193] In addition, the program allows phantom size to be adjusted to match patients of any weight or height. FOV can be freely adjusted relative to the patient.[193]

The program uses an Excel (Microsoft, Redmond, WA) spreadsheet for calculation of the total volume effective dose. Each line within the spreadsheet represents a single pulse of the scan. This means that a scan with 360 total pulses would have 360 lines in the spreadsheet. Within each line, the parameters of the machine and scan are entered. Projection represents the

numerical angle of that individual pulse. The software angle orientation relative to the patient is represented in figure 1.

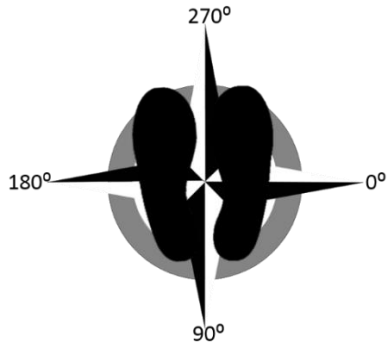

Figure 1: PCXMC angle orientation relative to patient

(As if looking up through the floor, so patient left is 0 degrees)

Considering the pathway of the source around the patient's head, the starting angle of the first pulse and the ending angle of the last pulse were entered on the first and last lines respectively, with all the remaining intermediate pulse angles entered on the remaining lines.

The number of scan pulses and all pulse angles were obtained from the manufacturers, either from the machine documentation themselves, or through direct inquiry. Patient height, weight, and age similar to the phantom used in the correlating physical scan were entered. PCXMC settings for an adult 30 year-old are 178.6 cm height and 73.2 kg weight, and the child setting for a 10 year old is 139.8 cm height and 32.4 kg weight. This is similar in external dimensions to the ATOM adult phantom (model 701-HN, CIRS, Norfolk, VA) which represents a 30 year old human of 173 cm height and 73 kg weight, and the ATOM child (model 706-HN, CIRS, Norfolk, VA), which represents a 10 year-old human of 140 cm and 32 kg. Machine filtration was entered in from the specific scanner product documentation. The FRD represents the distance between the x-ray source and the rotational reference point axis of the scan. This distance is found from product documentation or directly from the manufacturer. The x-ray beam width and height are calculated using the individual scan collimations, which create specific x-ray beam field dimensions at the receptor. The scan collimations are obtained from

product documentation or directly from the manufacturer. The width and height of the x-ray beam field at the reference axis are calculated from the x-ray beam field at the receptor using trigonometry. Given the dimensions of the field at the receptor, the x-ray beam may be considered a square pyramid, with the source as the apex. The height of the pyramid is the source to receptor distance, obtained either from machine documentation or directly from the manufacturer. As the dimensions of the base and height of the pyramid are known, the field of view at the reference axis can be calculated.

The x-ray tube voltage was entered from the parameters of the specific scan. The x, y, and z references are the coordinates of the center of the rectangular scan field at the reference axis. PCXMC has a simulated scout window, shown in figure 2, which allows visual placement of the scan relative to the patient. Each simulated scan is situated to replicate phantom scan placement. The input dose quantity chosen for this research was mAs and dose area product (DAP). Each machine provides both mAs and DAP for each scan protocol. For each scan, these are divided by the number of scan pulses for that scan, and entered under the category "input dose value," with the mAs per pulse on each line of the mAs scan, and the DAP per pulse on each line of the DAP scan. For each phantom scan protocol, one simulated scan was run using the mAs input value, and then another simulated scan using the DAP input value.

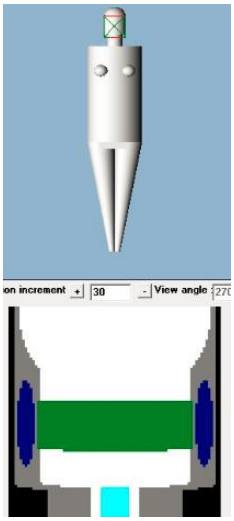

Figure 2: PCXMC Positioning and scout window

For the purpose of the mathematical evaluation, the program considers that the x-ray photons are emitted from a point source and then interact within the parameters specified in the scan (x-ray FOV size, patient reference axis, pulse angle, etc.). Pseudo-random numbers are generated to simulate photon direction, interaction distance, type of interacting atom, interaction type with that atom, scatter angle, and energy loss. These photons are then followed in their interactions in the phantom using the probability of types of scatter or photoelectric absorption.[193] The process of interactions is compiled to create a "photon history." Many independent photon histories are created, which then are used to estimate the energy deposited in the simulated organs of the phantom.[193]

From this information, the program calculates the effective dose using both ICRP 103 and 60 values. The sum of each line effective dose is taken, representing the effective dose of the entire scan. For this study, only ICRP 103 values were evaluated. PCXMC 2.0 was run on a laptop computer (Lenovo, Morrisville, NC and Beijing, China) using Windows 7 (Microsoft, Redmond, WA).

Dosimetry values were calculated using these parameters and compared with phantom dosimetry results. The null hypothesis, that there is no statistically significant difference between the dosimetry values of the anthropomorphic phantom and the calculated values of the PCXMC software, was tested.

Similar to previous studies, initial evaluation consisted of simple percent difference relative to the phantom measured dose.[196] The results (organ equivalent doses and total effective doses) were then categorized into a binary variable: positive if the estimated results were within ±20% of the phantom, and negative for everything else. All statistics were run using SPSS statistical software (IBM, Armonk, New York, USA). A chi-square test was performed comparing mAs versus DAP input variables on effective dose. Logistic regression was performed using the following variables relative to the binary effective dose: machine used, phantom used (adult or child), FOV location, FOV volume size, and phantom measured dose.

Due to the unitary data from the NewTom 3G, it was excluded from machine specific, but not global, comparisons. To evaluate equivalent dose among the different organs, another chi-square was completed.

RESULTS

The percent difference of the PCXMC estimated doses relative to the phantom doses are given in figure 3-figure 6.

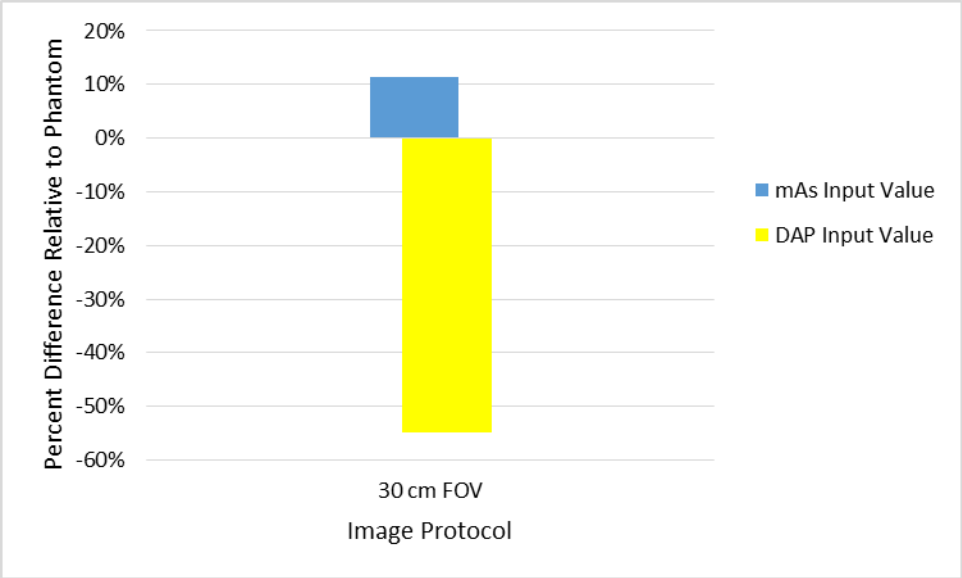

Figure 3: NewTom 3G PCXMC effective dose estimates relative to phantom

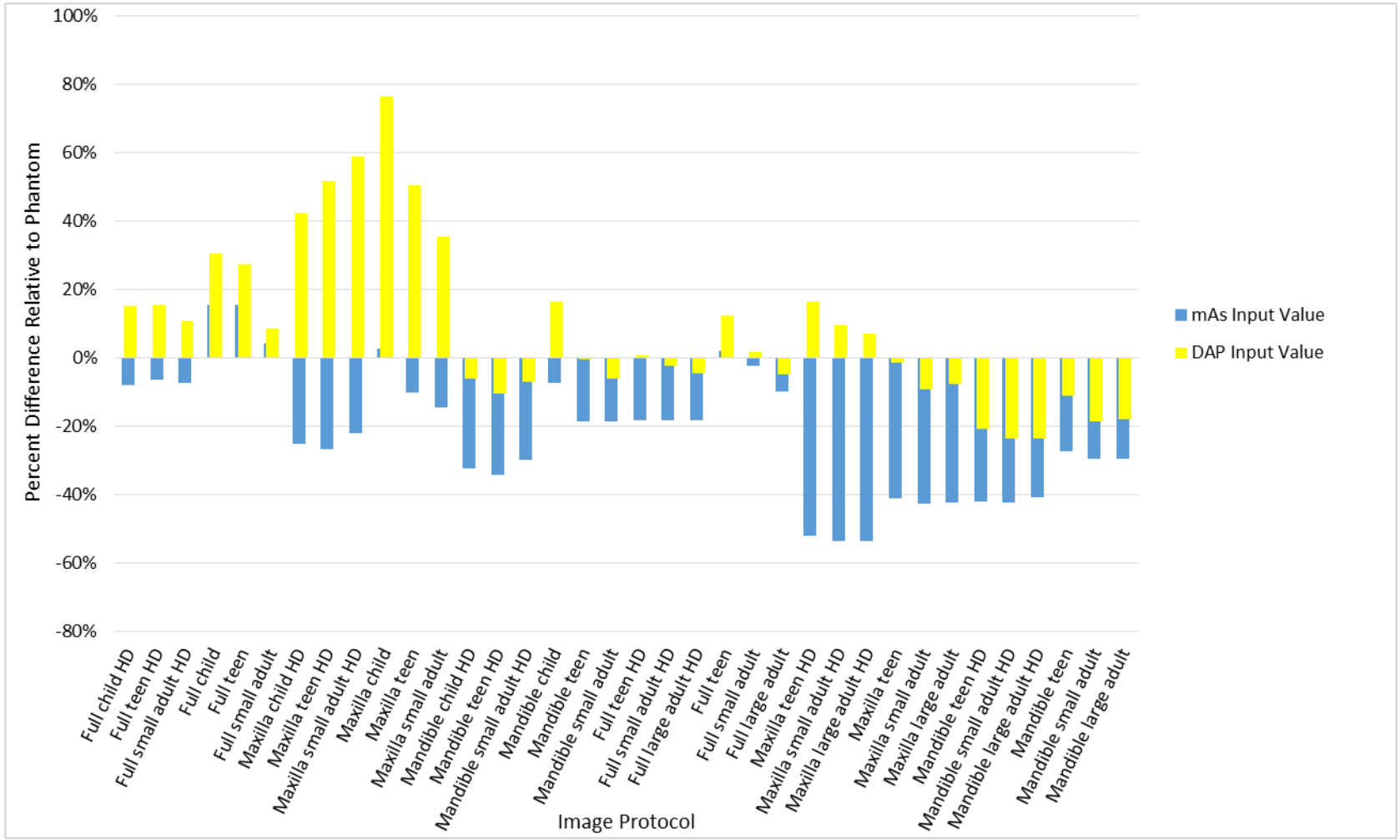

Figure 4: Sirona Galileos Comfort Plus PCXMC effective dose estimates relative to phantom

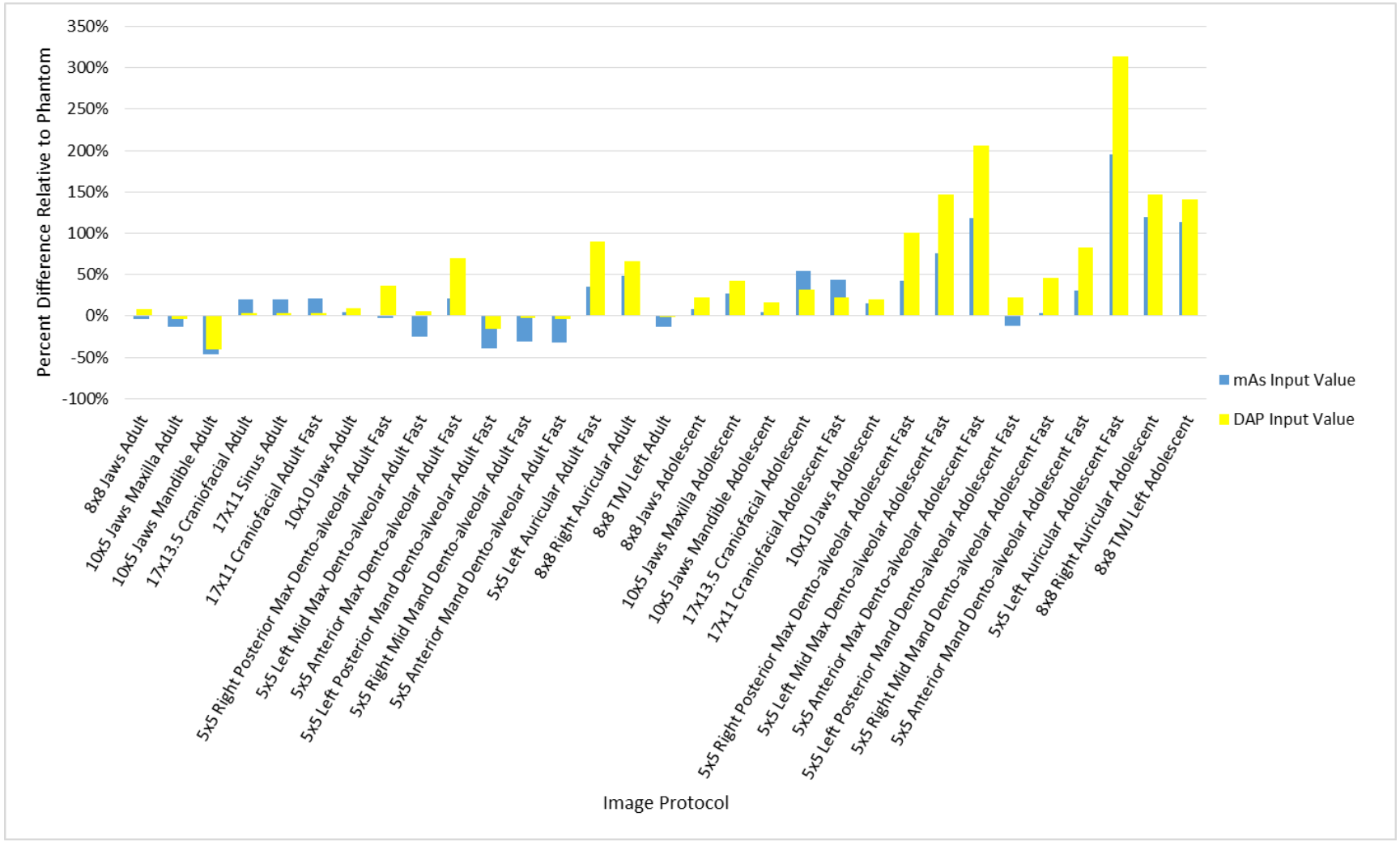

Figure 5: CS9300 PCXMC effective dose estimates relative to phantom

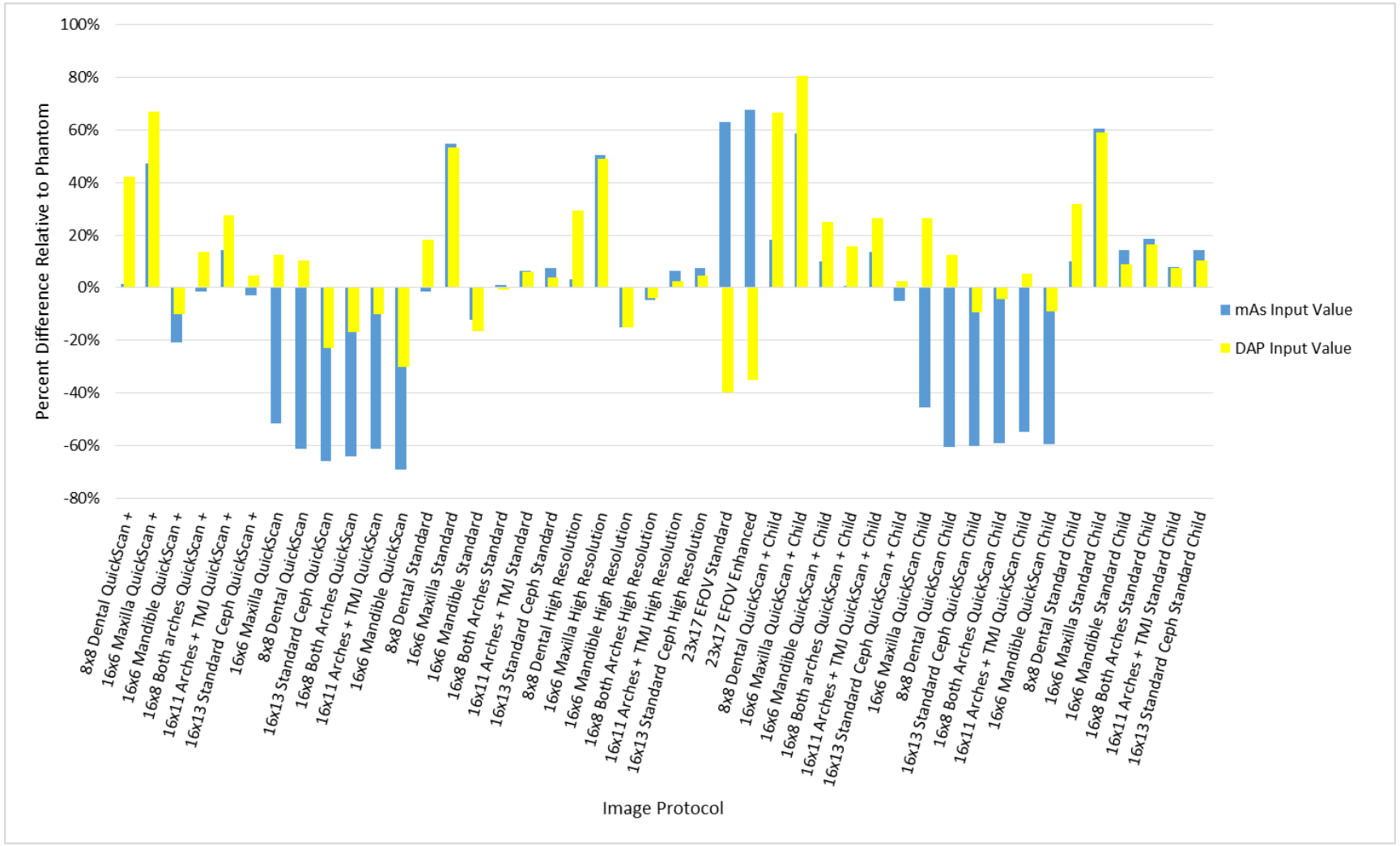

Figure 6: iCat FLX PCXMC effective dose estimates relative to phantom

Using mAs as the input variable resulted in simulated effective doses at or below the ±20% target threshold 48% of the time. Increasing the threshold to ±30% would result in 60% success, and to ±50%, 77% success. Using DAP as the input variable resulted in simulated effective doses at or below the ±20% threshold 57% of the time. Increasing that threshold to ±30% would result in 70% success, and to ±50%, 82% success. Differences were as much as 300% on the CS9300 for certain small FOVs. Even though there are visual percent differences between using mAs or DAP, the chi-square analysis showed there was not a significant association between input variable (mAs or DAP) and whether or not PCXMC predicted dose was within ±20% of the phantom measured effective dose $\chi 2$ (1)=1.791, p=.114.

The logistic regression results showed that the only consistently significant finding was FOV location. Those protocols strictly in the maxilla and above were less likely to stay below the target threshold, and those that encompassed both maxilla and mandible were more likely to stay below the target threshold. When mAs was used as the input variable, effective doses in larger volumes were slightly less likely to be below the target threshold. When DAP was used as the input variable, effective doses in the adult phantom were more likely to be below the target threshold. The results are shown in figure 7 and Figure 8.

Analysis of Maximum Likelihood Estimates (mAs)

Parameter		DF	Estimate	SE	Wald Chi-Square	Pr > ChiSq
Machine	CS9300	1	-0.1475	0.3429	0.1851	0.667
Machine	iCat FLX	1	0.3782	0.4128	0.8396	0.3595
Phantom Used	Adult	1	-0.5252	0.4698	1.2496	0.2636
Dose		1	-0.00338	0.00493	0.4701	0.493
FOV Location	Full	1	2.0433	0.4315	22.4212	<.0001
FOV Location	Maxilla	1	-1.5152	0.3899	15.1014	0.0001
FOV Volume (cm3)		1	-0.00089	0.00035	6.304	0.012

Figure 7: Logistic Regression with mAs as the input variable. Variables examined included machine used, phantom used (adult or child), FOV location, FOV volume size, and phantom measured dose

Analysis of Maximum Likelihood Estimates (DAP)

Parameter		DF	Estimate	SE	Wald Chi-Square	Pr > ChiSq
Machine	CS9300	1	-0.6237	0.3343	3.4804	0.0621
Machine	iCat FLX	1	-0.0098	0.3643	0.0007	0.9785
Phantom Used	Adult	1	1.4437	0.4695	9.4547	0.0021
Dose		1	0.00597	0.00548	1.1836	0.2766
FOV Location	Full	1	0.9107	0.3621	6.3241	0.0119
FOV Location	Maxilla	1	-1.2947	0.3583	13.0584	0.0003
FOV Volume (cm3)		1	-0.00027	0.000222	1.4429	0.2297

Figure 8: Logistic Regression with DAP as the input variable. Variables examined included machine used, phantom used (adult or child), FOV location, FOV volume size, and phantom measured dose.

The percentage of the software organ equivalent dose estimates that were within ±20% of the phantom measured doses are given in figure 9.

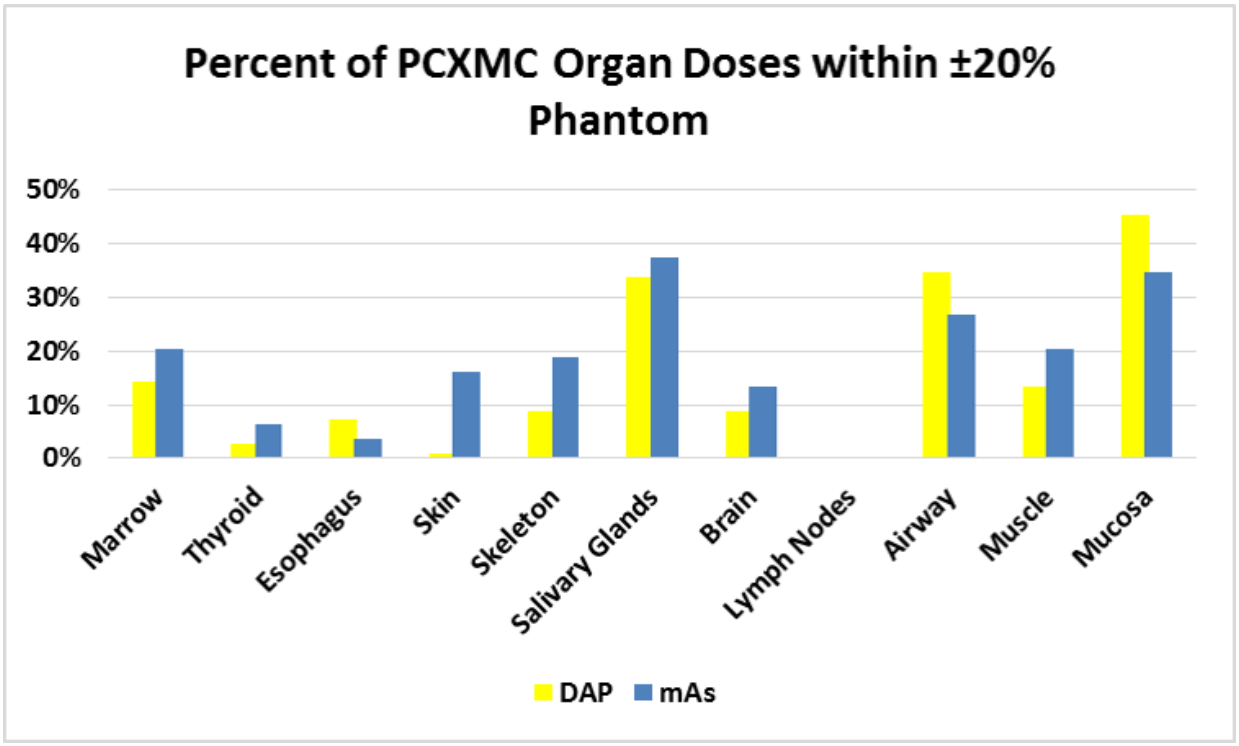

Figure 9: Percentage of PCXMC organ dose estimates within ±20% of phantom, with DAP or mAs as input variable.

In evaluating equivalent dose on the organs, the mucosa, salivary glands, and airway had the most estimates within the threshold using both mAs and DAP. Lymph nodes had none in both.

The chi-square analysis on the equivalent doses of all the organs shows that when using mAs as the input variable, there is a significant but only moderate association between the organ and whether the dose was within the phantom dose threshold ($\chi 2$ (9)=76.945, p<.001, Cramer's V= .262). Using DAP as the input variable, the association was slightly stronger ($\chi 2$ (9)=168.714, p<.001, Cramer's V= .388). Figure 10 and figure 11 show the standardized residuals. Positive and negative values represents greater than or less than expected counts, and the number value represents the significance. All other organs were not significant. (See Appendix 1 and 2)

Organ	Std. Residual
Salivary	4.2
Mucosa	3.6
Thyroid	-3.2
Esophagus	-3.9

Figure 10: Chi-square standardized residuals, with mAs as input value

Organ	Std. Residual
Mucosa	7.3
Airway	4.6
Salivary	4.3
Skeleton	-2.1
Brain	-2.1
Esophagus	-2.5
Thyroid	-3.7
Skin	-4.1

Figure 11: Chi-square standardized residuals, with DAP as input value

DISCUSSION

In evaluating of the significance of the FOV location, previous research has demonstrated that when organs are partially within the x-ray field, doses can drastically differ between phantoms.[197] While this doesn't explain why mandibular FOVs were not significantly different, it does logically follow that as more organs are partially within the scan, the more variance between phantoms is encountered.

However, this does not explain the only significant finding relating to FOV size. When using mAs as the input variable, larger FOVs were slightly less likely of being within 20% of the phantom measured effective dose. Logically, it follows that a smaller FOV would have more organs partially within the scan, and accordingly, greater variability. Other than the fact that the likelihood ratio is so small (-0.00089) that it may be statistically, but not practically significant, this finding cannot be explained at this time.

The variance in adult versus child phantom when using DAP is consistent with previous research, that found significant changes in effective dose without any change in DAP.[198] Additionally, studies have shown vast differences in conversion factors when attempting to equate DAP with effective dose.[165, 199] In the protocols that scanned both adult and child phantoms, DAP did not change between the two. Child phantom organ positioning may have an even greater effect on effective dose deviations in this instance, as more organs, particularly the thyroid, are included or proximal to the beam.[192] Differences in organ position can have significant effects on organ and equivalent dose.[200]

Limitations

Initial concerns were regarding the machine specific FOV geometry, since PCXMC calculates the scan as a cylinder. Two of the machines evaluated, the NewTom 3G and Galileos, have spherical FOVs, while the CS9300 and iCat FLX have a cylindrical FOVs. However, no significant difference was found between the machines themselves.

Additionally, as PCXMC allows for FOV placement in all three planes (X, Y, and Z) the positioning scan, particularly with smaller protocols, will always be a potential source of error. While a scout window is present within PCXMC, positioning still requires human judgment. To test this, software scans were run with several cm differences in positioning. Estimated effective dose from the software varied less than 5% with different positions, unless the exam bordered the thyroid. Greater inclusion of the thyroid within the scan by moving the target inferiorly increased the estimated effective dose upwards of 15%, with dramatic increases in equivalent dose to the organ itself. However, the potential variation is still present, and is illustrated in several 5x5 FOV protocols in the CS9300, which demonstrated some of the highest variation in this study, with differences ranging from 3% to above 200 and 300% difference from the phantom. PCXMC overestimated doses in 13 out of 14 instances. In this machine specific subset of imaging protocols, there was no consistency on location relative to percent difference (posterior/anterior FOV, or maxillary/mandibular FOV)

Another significant potential source of error is the choice of the phantom itself. There are a few different types of computational phantoms. The phantom used in PCXMC is a hermaphroditic, mathematical computational phantom, often called 'stylized,' 'mathematical' or 'MIRD-type,' since they were introduced by the Medical Internal Radiation Dose Committee (MIRD).[201] The internal organ structure and exterior tissue are described by three-dimensional surface equations.[202] This mathematical polyhedral method of representing organs can be considered simplistic compared to the complex anatomy of the human body, and as such, can introduce the potential for error in dose estimations.[202] Another group of computational

phantoms are “voxel” or “tomographic” phantoms. These phantoms use magnetic resonance (MR) or CT image information to construct organ and body structure.[202] A third recent type of computational phantom has been developed – called “hybrid” or “boundary representation” (BREP) phantoms.[184, 203] These phantoms have the benefit of being easily deformable – which allows the alteration to fit different organ shapes or different body types. These may be constructed with a polygonal mesh – a set of faces that determine the polyhedral shape of organs and other structures. These newer phantoms allow for simulation of particularly complex anatomies.[184]

The computational phantoms with more realistic anatomy have been compared to the initial stylized phantoms.[197, 203-207] Exposure levels in organs between certain phantoms (and classes of phantoms) can vary significantly, and relate to organ shape and distribution.[202, 207] Effective dose can depend strongly on the choice of phantom, organ positions, and field size and position.[200] The phantom used in PCXMC includes soft tissue, lung tissue, and skeleton. The ATOM phantom includes soft tissue, spinal cord, spinal disks, lung, brain, and sinus, and the RANDO phantom includes soft tissue, lungs, and natural human skeletons.[176, 177] Although phantom tissue attenuation factors aim to follow ICRP recommendations, there are natural variations between human bone and polymers, as well as inherent differences between systems.[177, 193] Even when comparing different phantoms of the same type (e.g. voxel phantoms with voxel phantoms), differences in effective dose have been found to range up to nearly 50%.[206] Of note is when there is inability to alter the orientation of the phantom head within the scan to more appropriately model patient head positioning. Since positioning within the scan has been shown to make a significant difference on organ and effective dose,[94, 96, 99, 198] this results in the fact that phantoms intended for general dosimetry may ultimately be limited and present with inherent variance when used in dental CBCT application.

PCXMC Previous Validation Studies

Studies comparing PCXMC with other Monte Carlo programs and phantoms have shown varying levels of agreement.[139, 197] In evaluating PCXMC with MCNP, a Monte Carlo program from the Los Alamos National Laboratory (LANL) Schultz and co-workers found that while the PCXMC estimated individual organ doses during pediatric cardiology procedures sometimes varied considerably from the MCNP values, effective dose had more reasonable agreement.[139] Since the effective doses evaluated were in mSv, the acceptable margin of error included differences of up to nearly 800 μSv.[139]

In comparing PCXMC with a voxel phantom and MCNPX (LANL, Los Alamos, NM), Smans and co-workers found increased differences in mean organ dose between phantoms when organs were partially within the x-ray field, as much as 700%.[197] Even when the different phantoms underwent total body irradiation, differences in mean organ doses between the phantoms ranged from 1%-96%.[197]

Previous studies have shown similar range of agreement with PCXMC effective dose estimations and other physical dose measurements.[139, 146, 193, 200, 208, 209] Schmidt and co-workers found that a comparison of PCXMC estimates with a list of doses from a selection of common cardiac projections for 1 Gy entrance air kerma was within 10-20%.[200] Effective doses in this comparison ranged from approximately 5-25mSv. The accepted percent variance of 20% difference of 20mSv correlates to 4 mSv, or 4,000 μSv, which is a 1300% difference from the maximum phantom calculated effective dose (less than 0.3 mSv, or 300 μSv) of the machines evaluated in this study. Khelassi-Toutaoui and co-workers compared PCXMC with PREPARE (ORNL, Oak Ridge, TN), another MC program against TLDs in a RANDO phantom during simulated lung exposures. The authors found that phantom measured doses correlated better with the PCXMC values than the PREPARE values. PCXMC organ dose values were within 28% in 60% of the samples.[209]

Another study by Helmrot and co-workers found that software estimated absorbed doses agreed within ±50% of measured absorbed doses to the uterus.[208] The difference between PCXMC estimates and measured absorbed dose in this study was commonly within the range of 0.1-0.2 mGy (100-200 μGy) and varied as much as 5mGy.[208] Wood and co-workers evaluated the CBCT dose associated with a Varian on-board-imager CBCT (OBI, Varian Medical Systems, Palo Alto, CA) against RANDO phantom TLDs. The authors found that the majority of software estimated organ doses were within 20%.[146] As the doses were in mGy, the smallest number difference was 0.3 mGy, or 300 μGy. Overall, even though PCXMC was shown to have reasonable agreement with the comparison phantoms, Monte Carlo programs, and other dose measurements, the acceptable difference margin in those studies often exceeded the largest doses evaluated within this present study.

Organ doses

The evaluation of PCXMC organ dose estimations should be approached with a caveat – as it is explicitly stated within software documentation that they are only strictly valid for phantoms used in the calculation.[193] Statistical analysis on the organs shows that while the organ does have a significant effect on being within the threshold dose, the association between the two is only low to medium in strength. Cramer's V, a measure of the association between organ and being within threshold dose, was .262 and .388 for mAs and DAP respectively. One key finding is that with both mAs and DAP, the thyroid had significantly less than expected hits within the phantom dose threshold (both $p < .001$, see Appendix 1 and 2). This is important as the thyroid, while on the periphery of most scans, contributes significantly to effective dose when it is scan adjacent. Specifically regarding the lymph nodes, PCXMC does not model the nodes themselves, but compiles a dose estimate from doses in surrogate organs, explained in figure 12.[193] This would explain the zero success rate – as the majority of organs within the compilation are far from the primary beam. In contrast, previous ATOM phantom dental CBCT

dosimetry accounts for lymph nodes by averaging from dosimeters near anatomical head and neck lymph node locations. Additionally, precision of the dose estimate may be low if the dose to the organ is low.[193] Common doses in dental CBCT are 10-1000 times less than those protocols used in studies cited previously. This primarily explains the low global success rate in organ dose estimation. This reiterates an important issue – since effective dose is compiled from organ doses, differences between phantoms can lead to significant variations in dose.

$$
\begin{aligned}
D_{\text{lymph nodes}} = {} & 0.25 \cdot D_{\text{small intestines}} + 0.15 \cdot D_{\text{pancreas}} + \\
& 0.13 \cdot D_{\text{extrathoracic airways}} + 0.10 \cdot D_{\text{gall bladder}} + \\
& 0.08 \cdot D_{\text{salivary glands}} + 0.07 \cdot D_{\text{lungs}} + \\
& 0.05 \cdot D_{\text{thyroid}} + 0.05 \cdot D_{\text{total body}} + \\
& 0.04 \cdot D_{\text{oesophagus}} + 0.04 \cdot D_{\text{heart}} + \\
& 0.03 \cdot D_{\text{stomach}} + 0.01 \cdot D_{\text{testes}} .
\end{aligned}
$$

Figure 12: PCXMC lymph node dose calculation

Dental CBCT Dose concerns: Are they worth discussing?

Since the dose levels of dental CBCT are generally low relative to medical diagnostic radiology protocols, are they even worth discussing? While certain individuals have stated that additional low level radiation exposure is beneficial to health,[210-213] reviews of any published literature has not been strongly supportive.[214, 215] Even among professional bodies there is continual discussion of dose levels and related risks. While in 2011, the American Association of Physicists in Medicine released a policy statement declaring that the "risks of medical imaging at effective doses below 50 mSv (50,000 μSv)…may be nonexistent",[216] other studies have found increased risks of leukemia and brain cancers at similar doses,[217, 218] and NCRP report #116 recommended that a negligible annual individual dose be considered as low as 0.01 mSv (10 μSv).[219] Individual dental CBCT scans are regularly above the NCRP recommended level. Even though the risk is extrapolated from higher doses and is small for an individual, applying this to

a population of patients results in a public health concern that cannot be deemed insignificant.[165] Thus, dental CBCT doses ARE worth discussing.

Future Directions

The idea of Monte Carlo analysis is to create a model that very closely simulates the real system, then calculate interactions.[188] As anthropomorphic phantoms have been shown to reliably measure effective dose with dental CBCT,[220] MC programs must act similarly in order to be a precise and accurate substitution. The utilization of programs with newer phantoms that: 1) more closely model human anatomy and 2) allow for realistic adjustment to match patient populations and 3) allow positioning to match dental patient imaging protocols may ultimately become the future of dental dosimetry.

CONCLUSIONS

PCXMC is not currently a generally acceptable substitution for the current standard of dental CBCT phantom dosimetry. A ±50% threshold relative to current phantom dosimetry is required for the program to be successful 80% of the time. While the software calculations are simpler to perform than anthropomorphic phantom dosimetry, simplicity is not an acceptable tradeoff for this level of imprecision in most applications.

APPENDIX 1: MAS INPUT VARIABLE ORGAN CHI-SQUARE ANALYSIS

Organs Coded * mAs Hit Threshold? Crosstabulation

			mAs Hit Threshold?		
			NO	YES	Total
Organs Coded	Marrow	Count	89	23	112
		Expected Count	89.8	22.2	112.0
		% within Organs Coded	79.5%	20.5%	100.0%
		% within mAs Hit Threshold?	9.9%	10.4%	10.0%
		% of Total	7.9%	2.1%	10.0%
		Std. Residual	-.1	.2	
	Thyroid	Count	105	7	112
		Expected Count	89.8	22.2	112.0
		% within Organs Coded	93.8%	6.3%	100.0%
		% within mAs Hit Threshold?	11.7%	3.2%	10.0%
		% of Total	9.4%	.6%	10.0%
		Std. Residual	1.6	-3.2	
	Esophagus	Count	108	4	112
		Expected Count	89.8	22.2	112.0
		% within Organs Coded	96.4%	3.6%	100.0%
		% within mAs Hit Threshold?	12.0%	1.8%	10.0%
		% of Total	9.6%	.4%	10.0%
		Std. Residual	1.9	-3.9	
	Skin	Count	94	18	112
		Expected Count	89.8	22.2	112.0
		% within Organs Coded	83.9%	16.1%	100.0%
		% within mAs Hit Threshold?	10.5%	8.1%	10.0%
		% of Total	8.4%	1.6%	10.0%
		Std. Residual	.4	-.9	
	Skeleton	Count	91	21	112
		Expected Count	89.8	22.2	112.0
		% within Organs Coded	81.3%	18.8%	100.0%
		% within mAs Hit Threshold?	10.1%	9.5%	10.0%

		% of Total	8.1%	1.9%	10.0%
		Std. Residual	.1	-.3	
	Salivary	Count	70	42	112
		Expected Count	89.8	22.2	112.0
		% within Organs Coded	62.5%	37.5%	100.0%
		% within mAs Hit Threshold?	7.8%	18.9%	10.0%
		% of Total	6.3%	3.8%	10.0%
		Std. Residual	-2.1	4.2	
	Brain	Count	97	15	112
		Expected Count	89.8	22.2	112.0
		% within Organs Coded	86.6%	13.4%	100.0%
		% within mAs Hit Threshold?	10.8%	6.8%	10.0%
		% of Total	8.7%	1.3%	10.0%
		Std. Residual	.8	-1.5	
	Airway	Count	82	30	112
		Expected Count	89.8	22.2	112.0
		% within Organs Coded	73.2%	26.8%	100.0%
		% within mAs Hit Threshold?	9.1%	13.5%	10.0%
		% of Total	7.3%	2.7%	10.0%
		Std. Residual	-.8	1.7	
	Muscle	Count	89	23	112
		Expected Count	89.8	22.2	112.0
		% within Organs Coded	79.5%	20.5%	100.0%
		% within mAs Hit Threshold?	9.9%	10.4%	10.0%
		% of Total	7.9%	2.1%	10.0%
		Std. Residual	-.1	.2	
	Mucosa	Count	73	39	112
		Expected Count	89.8	22.2	112.0
		% within Organs Coded	65.2%	34.8%	100.0%
		% within mAs Hit Threshold?	8.1%	17.6%	10.0%
		% of Total	6.5%	3.5%	10.0%
		Std. Residual	-1.8	3.6	
Total		Count	898	222	1120

	Expected Count	898.0	222.0	1120.0
	% within Organs Coded	80.2%	19.8%	100.0%
	% within mAs Hit Threshold?	100.0%	100.0%	100.0%
	% of Total	80.2%	19.8%	100.0%

Chi-Square Tests

	Value	df	Asymp. Sig. (2-sided)	Exact Sig. (2-sided)	Exact Sig. (1-sided)	Point Probability
Pearson Chi-Square	76.945[a]	9	.000	.000		
Likelihood Ratio	82.788	9	.000	.[b]		
Fisher's Exact Test	.[b]			.[b]		
Linear-by-Linear Association	26.943[c]	1	.000	.000	.000	.000
N of Valid Cases	1120					

a. 0 cells (0.0%) have expected count less than 5. The minimum expected count is 22.20.

b. Cannot be computed because there is insufficient memory.

c. The standardized statistic is 5.191.

Directional Measures

			Value	Asymp. Std. Error[a]	Approx. T[b]	Approx. Sig.	Exact Sig.
Nominal by Nominal	Lambda	Symmetric	.031	.013	2.353	.019	
		Organs Coded Dependent	.038	.016	2.353	.019	
		mAs Hit Threshold? Dependent	0.000	0.000	.[c]	.[c]	
	Goodman and Kruskal tau	Organs Coded Dependent	.008	.002		.000[d]	.000
		mAs Hit Threshold? Dependent	.069	.014		.000[d]	.[e]

a. Not assuming the null hypothesis.

b. Using the asymptotic standard error assuming the null hypothesis.

c. Cannot be computed because the asymptotic standard error equals zero.

d. Based on chi-square approximation

e. Cannot be computed because there is insufficient memory.

Symmetric Measures

		Value	Approx. Sig.	Exact Sig.
Nominal by Nominal	Phi	.262	.000	.000
	Cramer's V	.262	.000	.000
	Contingency Coefficient	.254	.000	.000
N of Valid Cases		1120		

APPENDIX 2: DAP INPUT VARIABLE ORGAN CHI-SQUARE ANALYSIS

Organs Coded * DAP Hit Threshold? Crosstabulation

			DAP Hit Threshold?		
			NO	YES	Total
Organs Coded	Marrow	Count	96	16	112
		Expected Count	92.9	19.1	112.0
		% within Organs Coded	85.7%	14.3%	100.0%
		% within DAP Hit Threshold?	10.3%	8.4%	10.0%
		% of Total	8.6%	1.4%	10.0%
		Std. Residual	.3	-.7	
	Thyroid	Count	109	3	112
		Expected Count	92.9	19.1	112.0
		% within Organs Coded	97.3%	2.7%	100.0%
		% within DAP Hit Threshold?	11.7%	1.6%	10.0%
		% of Total	9.7%	.3%	10.0%
		Std. Residual	1.7	-3.7	
	Esophagus	Count	104	8	112
		Expected Count	92.9	19.1	112.0
		% within Organs Coded	92.9%	7.1%	100.0%
		% within DAP Hit Threshold?	11.2%	4.2%	10.0%
		% of Total	9.3%	.7%	10.0%
		Std. Residual	1.2	-2.5	
	Skin	Count	111	1	112
		Expected Count	92.9	19.1	112.0
		% within Organs Coded	99.1%	.9%	100.0%
		% within DAP Hit Threshold?	11.9%	.5%	10.0%
		% of Total	9.9%	.1%	10.0%
		Std. Residual	1.9	-4.1	
	Skeleton	Count	102	10	112
		Expected Count	92.9	19.1	112.0
		% within Organs Coded	91.1%	8.9%	100.0%
		% within DAP Hit Threshold?	11.0%	5.2%	10.0%

		% of Total	9.1%	.9%	10.0%
		Std. Residual	.9	-2.1	
	Salivary	Count	74	38	112
		Expected Count	92.9	19.1	112.0
		% within Organs Coded	66.1%	33.9%	100.0%
		% within DAP Hit Threshold?	8.0%	19.9%	10.0%
		% of Total	6.6%	3.4%	10.0%
		Std. Residual	-2.0	4.3	
	Brain	Count	102	10	112
		Expected Count	92.9	19.1	112.0
		% within Organs Coded	91.1%	8.9%	100.0%
		% within DAP Hit Threshold?	11.0%	5.2%	10.0%
		% of Total	9.1%	.9%	10.0%
		Std. Residual	.9	-2.1	
	Airway	Count	73	39	112
		Expected Count	92.9	19.1	112.0
		% within Organs Coded	65.2%	34.8%	100.0%
		% within DAP Hit Threshold?	7.9%	20.4%	10.0%
		% of Total	6.5%	3.5%	10.0%
		Std. Residual	-2.1	4.6	
	Muscle	Count	97	15	112
		Expected Count	92.9	19.1	112.0
		% within Organs Coded	86.6%	13.4%	100.0%
		% within DAP Hit Threshold?	10.4%	7.9%	10.0%
		% of Total	8.7%	1.3%	10.0%
		Std. Residual	.4	-.9	
	Mucosa	Count	61	51	112
		Expected Count	92.9	19.1	112.0
		% within Organs Coded	54.5%	45.5%	100.0%
		% within DAP Hit Threshold?	6.6%	26.7%	10.0%
		% of Total	5.4%	4.6%	10.0%
		Std. Residual	-3.3	7.3	
Total		Count	929	191	1120

	Expected Count	929.0	191.0	1120.0
	% within Organs Coded	82.9%	17.1%	100.0%
	% within DAP Hit Threshold?	100.0%	100.0%	100.0%
	% of Total	82.9%	17.1%	100.0%

Chi-Square Tests

	Value	df	Asymp. Sig. (2-sided)	Exact Sig. (2-sided)	Exact Sig. (1-sided)	Point Probability
Pearson Chi-Square	168.714[a]	9	.000	.000		
Likelihood Ratio	168.875	9	.000	.[b]		
Fisher's Exact Test	.[b]			.[b]		
Linear-by-Linear Association	70.876[c]	1	.000	.000	.000	.000
N of Valid Cases	1120					

a. 0 cells (0.0%) have expected count less than 5. The minimum expected count is 19.10.

b. Cannot be computed because there is insufficient memory.

c. The standardized statistic is 8.419.

Directional Measures

			Value	Asymp. Std. Error[a]	Approx. T[b]	Approx. Sig.	Exact Sig.
Nominal by Nominal	Lambda	Symmetric	.042	.013	3.033	.002	
		Organs Coded Dependent	.050	.016	3.033	.002	
		DAP Hit Threshold? Dependent	0.000	0.000	.[c]	.[c]	
	Goodman and Kruskal tau	Organs Coded Dependent	.017	.002		.000[d]	.000
		DAP Hit Threshold? Dependent	.151	.022		.000[d]	.[e]

a. Not assuming the null hypothesis.

b. Using the asymptotic standard error assuming the null hypothesis.

c. Cannot be computed because the asymptotic standard error equals zero.

d. Based on chi-square approximation

e. Cannot be computed because there is insufficient memory.

Symmetric Measures

		Value	Approx. Sig.	Exact Sig.
Nominal by Nominal	Phi	.388	.000	.000
	Cramer's V	.388	.000	.000
	Contingency Coefficient	.362	.000	.000
N of Valid Cases		1120		

REFERENCES

1. Eckhardt R. Stan Ulam, John von Neumann, and the Monte Carlo method. Los Alamos Science 1987;15:131-37.

2. Ulam SM. Adventures of a mathematician. New York: Scribner; 1976.

3. Everett CJ, Ulam S. Multiplicative Systems: I. Proc Natl Acad Sci U S A 1948;34(8):403-5.

4. Metropolis N. The Beginning of the Monte Carlo Method. Los Alamos Science 1987;15:125-30.

5. Richtmyer Rv, J. Statistical Methods in Neutron Diffusion. Los Alamos: Los Alamos National Laboratory; 1947.

6. Metropolis N, Ulam S. The Monte Carlo method. J Am Stat Assoc 1949;44(247):335-41.

7. Kalos MW, PA. Monte Carlo Methods, 2nd Edition. 2nd Edition ed. Darmstadt, Federal Republic of Germany: Wiley-Blackwell; 2008.

8. Lux I, Koblinger L. Monte Carlo particle transport methods: neutron and photon calculations. Boca Raton: CRC Press; 1991.

9. Norris J. Markov Chains. Cambridge, United Kingdom: Cambridge University Press; 1998.

10. Draper NR. The Cambridge Dictionary of Statistics, Fourth Edition by B. S. Everitt, A. Skrondal. International Statistical Review 2011;79(2):273-74.

11. PubMed search "monte carlo". "http://www.ncbi.nlm.nih.gov/pubmed/?term=%22monte+carlo%22". 2015.

12. Rogers DW. Fifty years of Monte Carlo simulations for medical physics. Phys Med Biol 2006;51(13):R287-301.

13. Abuhaimed A, Martin CJ, Sankaralingam M, Gentle DJ. A Monte Carlo investigation of cumulative dose measurements for cone beam computed tomography (CBCT) dosimetry. Phys Med Biol 2015;60(4):1519-42.

14. Abuhaimed A, C JM, Sankaralingam M, D JG, McJury M. An assessment of the efficiency of methods for measurement of the computed tomography dose index (CTDI) for cone beam (CBCT) dosimetry by Monte Carlo simulation. Phys Med Biol 2014;59(21):6307-26.

15. Alaei P, Spezi E. Commissioning kilovoltage cone-beam CT beams in a radiation therapy treatment planning system. J Appl Clin Med Phys 2012;13(6):3971.

16. Teymurazyan A, Rowlands JA, Pang G. Monte Carlo simulation of a quantum noise limited Cerenkov detector based on air-spaced light guiding taper for megavoltage x-ray imaging. Med Phys 2014;41(4):041907.

17. Son K, Cho S, Kim JS, and co-workers. Evaluation of radiation dose to organs during kilovoltage cone-beam computed tomography using Monte Carlo simulation. J Appl Clin Med Phys 2014;15(2):4556.

18. Poirier Y, Kouznetsov A, Koger B, Tambasco M. Experimental validation of a kilovoltage x-ray source model for computing imaging dose. Med Phys 2014;41(4):041915.

19. McMillan K, McNitt-Gray M, Ruan D. Development and validation of a measurement-based source model for kilovoltage cone-beam CT Monte Carlo dosimetry simulations. Med Phys 2013;40(11):111907.

20. Fleckenstein J, Jahnke L, Lohr F, Wenz F, Hesser J. Development of a Geant4 based Monte Carlo Algorithm to evaluate the MONACO VMAT treatment accuracy. Z Med Phys 2013;23(1):33-45.

21. Ding GX, Munro P. Radiation exposure to patients from image guidance procedures and techniques to reduce the imaging dose. Radiother Oncol 2013;108(1):91-8.

22. Roberts DA, Hansen VN, Thompson MG, and co-workers. Kilovoltage energy imaging with a radiotherapy linac with a continuously variable energy range. Med Phys 2012;39(3):1218-26.

23. Qiu Y, Moiseenko V, Aquino-Parsons C, Duzenli C. Equivalent doses for gynecological patients undergoing IMRT or RapidArc with kilovoltage cone beam CT. Radiother Oncol 2012;104(2):257-62.

24. Pawlowski JM, Ding GX. A new approach to account for the medium-dependent effect in model-based dose calculations for kilovoltage x-rays. Phys Med Biol 2011;56(13):3919-34.

25. Kim S, Song H, Samei E, Yin FF, Yoshizumi TT. Computed tomography dose index and dose length product for cone-beam CT: Monte Carlo simulations. J Appl Clin Med Phys 2011;12(2):3395.

26. Kim S, Yoshizumi T, Toncheva G, and co-workers. Estimation of computed tomography dose index in cone beam computed tomography: MOSFET measurements and Monte Carlo simulations. Health Phys 2010;98(5):683-91.

27. Kim S, Yoshizumi TT, Toncheva G, Frush DP, Yin FF. Estimation of absorbed doses from paediatric cone-beam CT scans: MOSFET measurements and Monte Carlo simulations. Radiat Prot Dosimetry 2010;138(3):257-63.

28. Kim S, Yoo S, Yin FF, Samei E, Yoshizumi T. Kilovoltage cone-beam CT: comparative dose and image quality evaluations in partial and full-angle scan protocols. Med Phys 2010;37(7):3648-59.

29. Dobler B, Streck N, Klein E, and co-workers. Hybrid plan verification for intensity-modulated radiation therapy (IMRT) using the 2D ionization chamber array I'mRT MatriXX--a feasibility study. Phys Med Biol 2010;55(2):N39-55.

30. Ding A, Gu J, Trofimov AV, Xu XG. Monte Carlo calculation of imaging doses from diagnostic multidetector CT and kilovoltage cone-beam CT as part of prostate cancer treatment plans. Med Phys 2010;37(12):6199-204.

31. Wulff J, Ubrich F, Zink K. Comment on "Monte Carlo simulation of an x-ray volume imaging cone beam CT unit" [Med. Phys. 36, 127-136 (2009)]. Med Phys 2009;36(3):1039; author reply 40.

32. Spezi E, Downes P, Radu E, Jarvis R. Monte Carlo simulation of an x-ray volume imaging cone beam CT unit. Med Phys 2009;36(1):127-36.

33. Downes P, Jarvis R, Radu E, Kawrakow I, Spezi E. Monte Carlo simulation and patient dosimetry for a kilovoltage cone-beam CT unit. Med Phys 2009;36(9):4156-67.

34. Chow JC, Leung MK, Van Dyk J. Variations of lung density and geometry on inhomogeneity correction algorithms: a Monte Carlo dosimetric evaluation. Med Phys 2009;36(8):3619-30.

35. Chow JC. Cone-beam CT dosimetry for the positional variation in isocenter: a Monte Carlo study. Med Phys 2009;36(8):3512-20.

36. Gu J, Bednarz B, Xu XG, Jiang SB. Assessment of patient organ doses and effective doses using the VIP-Man adult male phantom for selected cone-beam CT imaging procedures during image guided radiation therapy. Radiat Prot Dosimetry 2008;131(4):431-43.

37. Ding GX, Duggan DM, Coffey CW. Accurate patient dosimetry of kilovoltage cone-beam CT in radiation therapy. Med Phys 2008;35(3):1135-44.

38. Chow JC, Leung MK, Islam MK, Norrlinger BD, Jaffray DA. Evaluation of the effect of patient dose from cone beam computed tomography on prostate IMRT using Monte Carlo simulation. Med Phys 2008;35(1):52-60.

39. Ding GX, Duggan DM, Coffey CW. Characteristics of kilovoltage x-ray beams used for cone-beam computed tomography in radiation therapy. Phys Med Biol 2007;52(6):1595-615.

40. Vanderstraeten B, Reynaert N, Paelinck L, and co-workers. Accuracy of patient dose calculation for lung IMRT: A comparison of Monte Carlo, convolution/superposition, and pencil beam computations. Med Phys 2006;33(9):3149-58.

41. Reynaert N, Coghe M, De Smedt B, and co-workers. The importance of accurate linear accelerator head modelling for IMRT Monte Carlo calculations. Phys Med Biol 2005;50(5):831-46.

42. Spezi E, Lewis DG, Smith CW. Monte Carlo simulation and dosimetric verification of radiotherapy beam modifiers. Phys Med Biol 2001;46(11):3007-29.

43. Francescon P, Cavedon C, Reccanello S, Cora S. Photon dose calculation of a three-dimensional treatment planning system compared to the Monte Carlo code BEAM. Med Phys 2000;27(7):1579-87.

44. Chytyk-Praznik K, VanUytven E, vanBeek TA, Greer PB, McCurdy BM. Model-based prediction of portal dose images during patient treatment. Med Phys 2013;40(3):031713.

45. Teymurazyan A, Pang G. Monte Carlo simulation of a novel water-equivalent electronic portal imaging device using plastic scintillating fibers. Med Phys 2012;39(3):1518-29.

46. van Elmpt W, Petit S, De Ruysscher D, Lambin P, Dekker A. 3D dose delivery verification using repeated cone-beam imaging and EPID dosimetry for stereotactic body radiotherapy of non-small cell lung cancer. Radiother Oncol 2010;94(2):188-94.

47. Haba T, Koyama S, Ida Y. Influence of difference in cross-sectional dose profile in a CTDI phantom on X-ray CT dose estimation: a Monte Carlo study. Radiol Phys Technol 2014;7(1):133-40.

48. Long DJ, Lee C, Tien C, and co-workers. Monte Carlo simulations of adult and pediatric computed tomography exams: validation studies of organ doses with physical phantoms. Med Phys 2013;40(1):013901.

49. Lee C, Kim KP, Long DJ, Bolch WE. Organ doses for reference pediatric and adolescent patients undergoing computed tomography estimated by Monte Carlo simulation. Med Phys 2012;39(4):2129-46.

50. Li X, Samei E, Segars WP, and co-workers. Patient-specific radiation dose and cancer risk estimation in CT: part II. Application to patients. Med Phys 2011;38(1):408-19.

51. Li X, Samei E, Segars WP, and co-workers. Patient-specific radiation dose and cancer risk estimation in CT: part I. development and validation of a Monte Carlo program. Med Phys 2011;38(1):397-407.

52. Zhang D, Savandi AS, Demarco JJ, and co-workers. Variability of surface and center position radiation dose in MDCT: Monte Carlo simulations using CTDI and anthropomorphic phantoms. Med Phys 2009;36(3):1025-38.

53. Turner AC, Zhang D, Kim HJ, and co-workers. A method to generate equivalent energy spectra and filtration models based on measurement for multidetector CT Monte Carlo dosimetry simulations. Med Phys 2009;36(6):2154-64.

54. Geleijns J, Salvado Artells M, de Bruin PW, and co-workers. Computed tomography dose assessment for a 160 mm wide, 320 detector row, cone beam CT scanner. Phys Med Biol 2009;54(10):3141-59.

55. Deak P, van Straten M, Shrimpton PC, Zankl M, Kalender WA. Validation of a Monte Carlo tool for patient-specific dose simulations in multi-slice computed tomography. Eur Radiol 2008;18(4):759-72.

56. DeMarco JJ, Cagnon CH, Cody DD, and co-workers. Estimating radiation doses from multidetector CT using Monte Carlo simulations: effects of different size voxelized patient models on magnitudes of organ and effective dose. Phys Med Biol 2007;52(9):2583-97.

57. DeMarco JJ, Cagnon CH, Cody DD, and co-workers. A Monte Carlo based method to estimate radiation dose from multidetector CT (MDCT): cylindrical and anthropomorphic phantoms. Phys Med Biol 2005;50(17):3989-4004.

58. Sawkey D, Lu M, Morin O, and co-workers. A diamond target for megavoltage cone-beam CT. Med Phys 2010;37(3):1246-53.

59. Wang Y, Antonuk LE, El-Mohri Y, and co-workers. Monte Carlo investigations of megavoltage cone-beam CT using thick, segmented scintillating detectors for soft tissue visualization. Med Phys 2008;35(1):145-58.

60. Monajemi TT, Fallone BG, Rathee S. Thick, segmented CdWO4-photodiode detector for cone beam megavoltage CT: a Monte Carlo study of system design parameters. Med Phys 2006;33(12):4567-77.

61. Mosleh-Shirazi MA, Swindell W, Evans PM. Optimization of the scintillation detector in a combined 3D megavoltage CT scanner and portal imager. Med Phys 1998;25(10):1880-90.

62. Bai M, Liu X, Liu B. Effective patient dose during neuroradiological C-arm CT procedures. Diagn Interv Radiol 2013;19(1):29-32.

63. Podnieks EC, Negus IS. Practical patient dosimetry for partial rotation cone beam CT. Br J Radiol 2012;85(1010):161-7.

64. Braak SJ, van Strijen MJ, van Es HW, Nievelstein RA, van Heesewijk JP. Effective dose during needle interventions: cone-beam CT guidance compared with conventional CT guidance. J Vasc Interv Radiol 2011;22(4):455-61.

65. Lanconelli N, Mettivier G, Lo Meo S, Russo P. Investigation of the dose distribution for a cone beam CT system dedicated to breast imaging. Phys Med 2013;29(4):379-87.

66. Mettivier G, Russo P, Lanconelli N, Meo SL. Cone-beam breast computed tomography with a displaced flat panel detector array. Med Phys 2012;39(5):2805-19.

67. Yi Y, Lai CJ, Han T, and co-workers. Radiation doses in cone-beam breast computed tomography: a Monte Carlo simulation study. Med Phys 2011;38(2):589-97.

68. Gomez-Ros JM, de Carlan L, Franck D, and co-workers. Monte Carlo modelling for in vivo measurements of Americium in a knee voxel phantom: general criteria for an international comparison. Radiat Prot Dosimetry 2007;127(1-4):245-8.

69. Zaidi H. Relevance of accurate Monte Carlo modeling in nuclear medical imaging. Med Phys 1999;26(4):574-608.

70. Jarry G, Graham SA, Moseley DJ, and co-workers. Characterization of scattered radiation in kV CBCT images using Monte Carlo simulations. Med Phys 2006;33(11):4320-9.

71. Malusek A, Seger MM, Sandborg M, Alm Carlsson G. Effect of scatter on reconstructed image quality in cone beam computed tomography: evaluation of a scatter-reduction optimisation function. Radiat Prot Dosimetry 2005;114(1-3):337-40.

72. Petoussi-Henss N, Zankl M, Drexler G, Panzer W, Regulla D. Calculation of backscatter factors for diagnostic radiology using Monte Carlo methods. Phys Med Biol 1998;43(8):2237-50.

73. Chin DW, Treister N, Friedland B, and co-workers. Effect of dental restorations and prostheses on radiotherapy dose distribution: a Monte Carlo study. J Appl Clin Med Phys 2009;10(1):2853.

74. Friedrich RE, Todorovic M, Heiland M, Scheuer HA, Krull A. Scattering effects of irradiation on surroundings calculated for a small dental implant. Anticancer Res 2012;32(5):2043-6.

75. Friedrich RE, Todorovic M, Krull A. Simulation of scattering effects of irradiation on surroundings using the example of titanium dental implants: a Monte Carlo approach. Anticancer Res 2010;30(5):1727-30.

76. Shimozato T, Igarashi Y, Itoh Y, and co-workers. Scattered radiation from dental metallic crowns in head and neck radiotherapy. Phys Med Biol 2011;56(17):5525-34.

77. Shishkina EA, Lyubashevskii NM, Tolstykh EI, and co-workers. A mathematical model for calculation of 90Sr absorbed dose in dental tissues: elaboration and comparison to EPR measurements. Appl Radiat Isot 2001;55(3):363-74.

78. Eskandarlou A, Jafari AA, Mohammadi M, and co-workers. Impact of rare earth element added filters on the X-ray beam spectra: a Monte Carlo approach. J Xray Sci Technol 2014;22(4):459-70.

79. Ivannikov AI, Tikunov DD, Borysheva NB, and co-workers. Calibration of EPR signal dose response of tooth enamel to photons: experiment and Monte Carlo simulation. Radiat Prot Dosimetry 2004;108(4):303-15.

80. Kovacs M, Danyi R, Erdelyi M, Fejerdy P, Dobo-Nagy C. Distortional effect of beam-hardening artefacts on microCT: a simulation study based on an in vitro caries model. Oral Surg Oral Med Oral Pathol Oral Radiol Endod 2009;108(4):591-9.

81. van der Veen MH, Ando M, Stookey GK, de Josselin de Jong E. A Monte Carlo simulation of the influence of sound enamel scattering coefficient on lesion visibility in light-induced fluorescence. Caries Res 2002;36(1):10-8.

82. Lee B, Lee J, Kang S, and co-workers. Calculation of patient effective dose and scattered dose for dental mobile fluoroscopic equipment: application of the Monte Carlo simulation. Radiat Prot Dosimetry 2013;153(1):80-4.

83. Tennant M, Kruger E. A dental public health approach based on computational mathematics: Monte Carlo simulation of childhood dental decay. Int Dent J 2013;63(1):39-42.

84. Aps JK, Scott JM. Oblique lateral radiographs and bitewings; estimation of organ doses in head and neck region with Monte Carlo calculations. Dentomaxillofac Radiol 2014;43(6):20130419.

85. Batista WO, Navarro MV, Maia AF. Effective doses in panoramic images from conventional and CBCT equipment. Radiat Prot Dosimetry 2012;151(1):67-75.

86. Lee B, Shin G, Kang S, and co-workers. Dose evaluation of selective collimation effect in cephalography by measurement and Monte Carlo simulation. Radiat Prot Dosimetry 2012;148(1):58-64.

87. Nicopoulou-Karayianni K, Koligliatis T, Donta-Bakogianni C, Karayiannis A, Litsas J. Radiation absorbed doses at compact bone-titanium interfaces in diagnostic radiography: a Monte Carlo approach. Dentomaxillofac Radiol 2003;32(5):327-32.

88. Walker C, van der Putten W. Patient dosimetry and a novel approach to establishing Diagnostic Reference Levels in dental radiology. Phys Med 2012;28(1):7-12.

89. Pujol A, Jr., Gibbs SJ. A Monte Carlo method for patient dosimetry from dental X-ray. Dentomaxillofac Radiol 1982;11(1):25-33.

90. Gibbs SJ, Pujol A, Jr., Chen TS, Malcolm AW, James AE, Jr. Patient risk from interproximal radiography. Oral Surg Oral Med Oral Pathol 1984;58(3):347-54.

91. Gibbs SJ, Pujol A, Jr., Chen TS, and co-workers. Radiation doses to sensitive organs from intraoral dental radiography. Dentomaxillofac Radiol 1987;16(2):67-77.

92. Gibbs SJ. Influence of organs in the ICRP's remainder on effective dose equivalent computed for diagnostic radiation exposures. Health Phys 1989;56(4):515-20.

93. Gibbs SJ. Effective dose equivalent and effective dose: comparison for common projections in oral and maxillofacial radiology. Oral Surg Oral Med Oral Pathol Oral Radiol Endod 2000;90(4):538-45.

94. Koivisto J, Kiljunen T, Tapiovaara M, Wolff J, Kortesniemi M. Assessment of radiation exposure in dental cone-beam computerized tomography with the use of metal-oxide semiconductor field-effect transistor (MOSFET) dosimeters and Monte Carlo simulations. Oral Surg Oral Med Oral Pathol Oral Radiol 2012;114(3):393-400.

95. Morant JJ, Salvado M, Casanovas R, and co-workers. Validation of a Monte Carlo simulation for dose assessment in dental cone beam CT examinations. Phys Med 2012;28(3):200-9.

96. Morant JJ, Salvado M, Hernandez-Giron I, and co-workers. Dosimetry of a cone beam CT device for oral and maxillofacial radiology using Monte Carlo techniques and ICRP adult reference computational phantoms. Dentomaxillofac Radiol 2013;42(3):92555893.

97. Vassileva J, Stoyanov D. Quality control and patient dosimetry in dental cone beam CT. Radiat Prot Dosimetry 2010;139(1-3):310-2.

98. Zhang G, Pauwels R, Marshall N, and co-workers. Development and validation of a hybrid simulation technique for cone beam CT: application to an oral imaging system. Phys Med Biol 2011;56(18):5823-43.

99. Zhang G, Marshall N, Bogaerts R, Jacobs R, Bosmans H. Monte Carlo modeling for dose assessment in cone beam CT for oral and maxillofacial applications. Med Phys 2013;40(7):072103.

100. Ludlow JB, Ivanovic M. Comparative dosimetry of dental CBCT devices and 64-slice CT for oral and maxillofacial radiology. Oral Surg Oral Med Oral Pathol Oral Radiol Endod 2008;106(1):106-14.

101. Ludlow JB, Davies-Ludlow LE, Brooks SL, Howerton WB. Dosimetry of 3 CBCT devices for oral and maxillofacial radiology: CB Mercuray, NewTom 3G and i-CAT. Dentomaxillofac Radiol 2006;35(4):219-26.

102. Koivisto J, Kiljunen T, Wolff J, Kortesniemi M. Characterization of MOSFET dosimeter angular dependence in three rotational axes measured free-in-air and in soft-tissue equivalent material. J Radiat Res 2013;54(5):943-9.

103. Davies J, Johnson B, Drage N. Effective doses from cone beam CT investigation of the jaws. Dentomaxillofac Radiol 2012;41(1):30-6.

104. Hansen J, Jurik AG, Fiirgaard B, Egund N. Optimisation of scoliosis examinations in children. Pediatr Radiol 2003;33(11):752-65.

105. Dragusin O, Gewillig M, Desmet W, and co-workers. Radiation dose survey in a paediatric cardiac catheterisation laboratory equipped with flat-panel detectors. Radiat Prot Dosimetry 2008;129(1-3):91-5.

106. Gialousis GI, Yakoumakis EN, Dimitriadis AI, and co-workers. Monte Carlo estimation of radiation doses in red bone marrow and breast in common pediatric x-ray examinations. Health Phys 2008;95(3):331-6.

107. Seidenbusch MC, Regulla D, Schneider K. [Radiation exposure of children in pediatric radiology. Part 3: Conversion coefficients for reconstruction of organ doses achieved during chest X-ray examinations]. Rofo 2008;180(12):1061-81.

108. Seidenbusch MC, Regulla D, Schneider K. [Radiation exposure of children in pediatric radiology--part 2: the PAEDOS algorithm for computer-assisted dose reconstruction in pediatric radiology and results for X-ray examinations of the skull]. Rofo 2008;180(6):522-39.

109. Seidenbusch MC, Regulla D, Schneider K. [Radiation exposure of children in pediatric radiology. Part 6: conversion factors for reconstruction of organ dose in abdominal radiography]. Rofo 2009;181(10):945-61.

110. Seidenbusch MC, Regulla D, Schneider K. [Radiation exposure of children in pediatric radiology. Part 7: conversion factors for reconstruction of organ dose during thoracoabdominal babygrams]. Rofo 2010;182(5):415-21.

111. Mogaadi M, Ben Omrane L, Hammou A. Effective dose for scoliosis patients undergoing full spine radiography. Radiat Prot Dosimetry 2012;149(3):297-303.

112. Beck NA, Miller R, Baldwin K, and co-workers. Do oblique views add value in the diagnosis of spondylolysis in adolescents? J Bone Joint Surg Am 2013;95(10):e65.

113. Kawasaki T, Aoyama T, Yamauchi-Kawaura C, Fujii K, Koyama S. Organ dose and effective dose estimation in paediatric chest radiographic examinations by using pin silicon photodiode dosemeters. Radiat Prot Dosimetry 2013;154(3):314-9.

114. Ma H, Elbakri IA, Reed M. Estimation of organ and effective doses from newborn radiography of the chest and abdomen. Radiat Prot Dosimetry 2013;156(2):160-7.

115. Vult von Steyern K, Bjorkman-Burtscher IM, Geijer M, Weber L. Conversion factors for estimation of effective dose in paediatric chest tomosynthesis. Radiat Prot Dosimetry 2013;157(2):206-13.

116. Yakoumakis E, Dimitriadis A, Makri T, and co-workers. Verification of radiation dose calculations during paediatric cystourethrography examinations using MCNP5 and PCXMC 2.0 Monte Carlo codes. Radiat Prot Dosimetry 2013;157(3):355-62.

117. Yakoumakis E, Kostopoulou H, Makri T, and co-workers. Estimation of radiation dose and risk to children undergoing cardiac catheterization for the treatment of a congenital heart disease using Monte Carlo simulations. Pediatr Radiol 2013;43(3):339-46.

118. Barnaoui S, Rehel JL, Baysson H, and co-workers. Local reference levels and organ doses from pediatric cardiac interventional procedures. Pediatr Cardiol 2014;35(6):1037-45.

119. Elbakri IA. Estimation of dose-area product-to-effective dose conversion factors for neonatal radiography using PCXMC. Radiat Prot Dosimetry 2014;158(1):43-50.

120. Parmaksiz A, Atac GK, Bulgurlu F, and co-workers. Unintentional irradiation of conceptus by diagnostic imaging examinations in Turkey. Radiat Prot Dosimetry 2014;162(3):322-8.

121. Peters M, Krings G, Koster M, and co-workers. Effective radiation dosage of three-dimensional rotational angiography in children. Europace 2014.

122. Sarkissian EJ, Sankar WN, Zhu X, Wu CH, Flynn JM. Radiographic Follow-up of DDH in Infants: Are X-rays Necessary After a Normalized Ultrasound? J Pediatr Orthop 2014.

123. Seidenbusch M, Schneider K. Conversion coefficients for determining organ doses in paediatric spine radiography. Pediatr Radiol 2014;44(4):434-56.

124. Seidenbusch MC, Harder D, Regulla DF, Schneider K. Conversion factors for determining organ doses received by paediatric patients in high-resolution single slice computed tomography with narrow collimation. Z Med Phys 2014;24(2):123-37.

125. Seidenbusch MC, Schneider K. Conversion coefficients for determining organ doses in paediatric pelvis and hip joint radiography. Pediatr Radiol 2014;44(9):1110-23.

126. Yakoumakis E, Dimitriadis A, Gialousis G, and co-workers. Evaluation of organ and effective doses during paediatric barium meal examinations using PCXMC 2.0 Monte Carlo code. Radiat Prot Dosimetry 2015;163(2):202-9.

127. Arbique GM, Gilleran JP, Guild JB, and co-workers. Radiation exposure during standing voiding cystourethrography in women. Urology 2006;67(2):269-74.

128. Gosch D, Gosch K, Kahn T. [Conversion coefficients for estimation of effective dose to patients from dose area product during fluoroscopy x-ray examinations]. Rofo 2007;179(10):1035-42.

129. Gyekye PK, Schandorf C, Boadu M, Yeboah J, Amoako JK. Patient dose assessment due to fluoroscopic exposure for some selected fluoroscopic procedures in Ghana. Radiat Prot Dosimetry 2009;136(3):203-8.

130. Yamamoto K, Azuma M, Kuroda C, and co-workers. Radiation dose in mass screening for gastric cancer with high-concentration barium sulfate compared with moderate-concentration barium sulfate. Australas Phys Eng Sci Med 2009;32(2):88-91.

131. Berner K, Bath M, Jonasson P, and co-workers. Dose optimisation of double-contrast barium enema examinations. Radiat Prot Dosimetry 2010;139(1-3):388-92.

132. Puustinen L, Numminen K, Uusi-Simola J, Sipponen T. Radiation exposure during nasojejunal intubation for MRI enteroclysis. Scand J Gastroenterol 2012;47(6):658-61.

133. Giarenis I, Phillips J, Mastoroudes H, and co-workers. Radiation exposure during videourodynamics in women. Int Urogynecol J 2013;24(9):1547-51.

134. D'Alessio D, Giliberti C, Soriani A, and co-workers. Dose evaluation for skin and organ in hepatocellular carcinoma during angiographic procedure. J Exp Clin Cancer Res 2013;32:81.

135. Gosch D, Kurze W, Deckert F, and co-workers. [Radiation exposure with 3D rotational angiography of the skull]. Rofo 2006;178(9):880-5.

136. Bogaert E, Bacher K, Thierens H. Interventional cardiovascular procedures in Belgium: effective dose and conversion factors. Radiat Prot Dosimetry 2008;129(1-3):77-82.

137. Dauer LT, Thornton R, Boylan DC, and co-workers. Organ and effective dose estimates for patients undergoing hepatic arterial embolization for treatment of liver malignancy. Med Phys 2011;38(2):736-42.

138. Peruzzo Cornetto A, Pasquino M, Aimonetto S, and co-workers. Interventional radiology at a single institution over 9 years: a comprehensive evaluation of procedures and an estimation of collective effective dose. J Vasc Interv Radiol 2012;23(12):1665-75.e2.

139. Schultz FW, Geleijns J, Spoelstra FM, Zoetelief J. Monte Carlo calculations for assessment of radiation dose to patients with congenital heart defects and to staff during cardiac catheterizations. Br J Radiol 2003;76(909):638-47.

140. Astroza GM, Neisius A, Wang AJ, and co-workers. Radiation exposure in the follow-up of patients with urolithiasis comparing digital tomosynthesis, non-contrast CT, standard KUB, and IVU. J Endourol 2013;27(10):1187-91.

141. Bath M, Svalkvist A, von Wrangel A, Rismyhr-Olsson H, Cederblad A. Effective dose to patients from chest examinations with tomosynthesis. Radiat Prot Dosimetry 2010;139(1-3):153-8.

142. Nelson G, Yoon S, Krishna G, Wilfley B, Fahrig R. Patient dose simulations for scanning-beam digital x-ray tomosynthesis of the lungs. Med Phys 2013;40(11):111917.

143. Svalkvist A, Mansson LG, Bath M. Monte Carlo simulations of the dosimetry of chest tomosynthesis. Radiat Prot Dosimetry 2010;139(1-3):144-52.

144. Alvarado R, Booth JT, Bromley RM, Gustafsson HB. An investigation of image guidance dose for breast radiotherapy. J Appl Clin Med Phys 2013;14(3):4085.

145. Ng JA, Booth J, Poulsen P, Kuncic Z, Keall PJ. Estimation of effective imaging dose for kilovoltage intratreatment monitoring of the prostate position during cancer radiotherapy. Phys Med Biol 2013;58(17):5983-96.

146. Wood TJ, Moore CS, Saunderson JR, Beavis AW. Validation of a technique for estimating organ doses for kilovoltage cone-beam CT of the prostate using the PCXMC 2.0 patient dose calculator. J Radiol Prot 2015;35(1):153-63.

147. Chen TR, Tyan YS, Chu CH, Wu MC, Tung CJ. Surveyed data for structural shielding calculations of radiographic x-ray installations in Taiwan. Health Phys 2013;104(5 Suppl 2):S60-7.

148. Poletti J. The effect of source to image distance on radiation risk to the patient. Australas Phys Eng Sci Med 2003;26(3):110-4.

149. Poletti JL, McLean D. The effect of source to image-receptor distance on effective dose for some common X-ray projections. Br J Radiol 2005;78(933):810-5.

150. Bogaert E, Bacher K, Thierens H. A large-scale multicentre study in Belgium of dose area product values and effective doses in interventional cardiology using contemporary X-ray equipment. Radiat Prot Dosimetry 2008;128(3):312-23.

151. Datz H, Ben-Shlomo A, Bader D, and co-workers. The additional dose to radiosensitive organs caused by using under-collimated X-ray beams in neonatal intensive care radiography. Radiat Prot Dosimetry 2008;130(4):518-24.

152. Baldelli P, Taibi A, Tuffanelli A, Gambaccini M. Dose comparison between conventional and quasi-monochromatic systems for diagnostic radiology. Phys Med Biol 2004;49(17):4135-46.

153. He W, Huda W, Magill D, Tavrides E, Yao H. Patient doses and projection angle in cone beam CT. Med Phys 2010;37(5):2359-68.

154. He W, Huda W, Magill D, Tavrides E, Yao H. X-ray tube current modulation and patient doses in chest CT. Radiat Prot Dosimetry 2011;143(1):81-7.

155. Glasser O. Wilhelm Conrad Röntgen and the Early History of the Roentgen Rays: Norman Pub.; 1993.

156. Hallikainen D. History of panoramic radiography. Acta Radiol 1996;37(3 Pt 2):441-5.

157. Hatcher DC. Operational principles for cone-beam computed tomography. J Am Dent Assoc 2010;141 Suppl 3:3s-6s.

158. Rigolone M, Pasqualini D, Bianchi L, Berutti E, Bianchi SD. Vestibular surgical access to the palatine root of the superior first molar: "low-dose cone-beam" CT analysis of the pathway and its anatomic variations. J Endod 2003;29(11):773-5.

159. Nakagawa Y, Kobayashi K, Ishii H, and co-workers. Preoperative application of limited cone beam computerized tomography as an assessment tool before minor oral surgery. Int J Oral Maxillofac Surg 2002;31(3):322-6.

160. Hamada Y, Kondoh T, Noguchi K, and co-workers. Application of limited cone beam computed tomography to clinical assessment of alveolar bone grafting: a preliminary report. Cleft Palate Craniofac J 2005;42(2):128-37.

161. Ogawa T, Enciso R, Memon A, Mah JK, Clark GT. Evaluation of 3D airway imaging of obstructive sleep apnea with cone-beam computed tomography. Stud Health Technol Inform 2005;111:365-8.

162. Tsiklakis K, Syriopoulos K, Stamatakis HC. Radiographic examination of the temporomandibular joint using cone beam computed tomography. Dentomaxillofac Radiol 2004;33(3):196-201.

163. Sato S, Arai Y, Shinoda K, Ito K. Clinical application of a new cone-beam computerized tomography system to assess multiple two-dimensional images for the preoperative treatment planning of maxillary implants: case reports. Quintessence Int 2004;35(7):525-8.

164. Hatcher DC, Dial C, Mayorga C. Cone beam CT for pre-surgical assessment of implant sites. J Calif Dent Assoc 2003;31(11):825-33.

165. Ludlow JB, Timothy R, Walker C, and co-workers. Effective dose of dental CBCT-a meta analysis of published data and additional data for nine CBCT units. Dentomaxillofac Radiol 2015;44(1):20140197.

166. Kau CH, Bozic M, English J, and co-workers. Cone-beam computed tomography of the maxillofacial region--an update. Int J Med Robot 2009;5(4):366-80.

167. White SC, Pharoah J. Oral Radiology: Principles and Interpretation: Mosby/Elsevier; 2009.

168. Bushong SC. Radiologic Science for Technologists: Physics, Biology, and Protection: Elsevier - Health Sciences Division; 2012.

169. Schauer DA, Linton OW. National Council on Radiation Protection and Measurements report shows substantial medical exposure increase. Radiology 2009;253(2):293-6.

170. Mettler FA, Jr., Thomadsen BR, Bhargavan M, and co-workers. Medical radiation exposure in the U.S. in 2006: preliminary results. Health Phys 2008;95(5):502-7.

171. Farman AG. ALARA still applies. Oral Surg Oral Med Oral Pathol Oral Radiol Endod 2005;100(4):395-7.

172. Lorenzoni DC, Bolognese AM, Garib DG, Guedes FR, Sant'anna EF. Cone-beam computed tomography and radiographs in dentistry: aspects related to radiation dose. Int J Dent 2012;2012:813768.

173. Image Wisely Campaign. American College of Radiology, Radiology Society of North America. "http://www.imagewisely.org/". 2015.

174. The Consortium of Computational Human Phantoms. The Consortium of Computational Human Phantoms. "http://www.virtualphantoms.org/phantoms.htm". 2015.

175. Alderson SW, Lanzl LH, Rollins M, Spira J. An instrumented phantom system for analog computation of treatment plans. Am J Roentgenol Radium Ther Nucl Med 1962;87:185-95.

176. The Phantom Laboratory. "http://phantomlab.com/products/rando.php". 2015.

177. Computerized Imaging Referencing System. "http://cirsinc.com/". 2015.

178. Kyoto Kagaku Ltd. "https://www.kyotokagaku.com/". 2015.

179. Griffith RV, Dean PN, Anderson AL, Fisher JC. Fabrication of a tissue-equivalent torso phantom for intercalibration of in-vivo transuranic-nuclide counting facilities; 1978.

180. Kim JI, Choi H, Lee BI, and co-workers. Physical phantom of typical Korean male for radiation protection purpose. Radiat Prot Dosimetry 2006;118(1):131-6.

181. Kramer GH, Burns L, Noel L. The BRMD BOMAB phantom family. Health Phys 1991;61(6):895-902.

182. Jones AK, Simon TA, Bolch WE, Holman MM, Hintenlang DE. Tomographic physical phantom of the newborn child with real-time dosimetry I. Methods and techniques for construction. Med Phys 2006;33(9):3274-82.

183. Staton RJ, Jones AK, Lee C, and co-workers. A tomographic physical phantom of the newborn child with real-time dosimetry. II. Scaling factors for calculation of mean organ dose in pediatric radiography. Med Phys 2006;33(9):3283-9.

184. Cassola VF, Lima VJ, Kramer R, Khoury HJ. FASH and MASH: female and male adult human phantoms based on polygon mesh surfaces: I. Development of the anatomy. Phys Med Biol 2010;55(1):133-62.

185. Kim CH, Jeong JH, Bolch WE, Cho KW, Hwang SB. A polygon-surface reference Korean male phantom (PSRK-Man) and its direct implementation in Geant4 Monte Carlo simulation. Phys Med Biol 2011;56(10):3137-61.

186. Winslow JF, Hyer DE, Fisher RF, Tien CJ, Hintenlang DE. Construction of anthropomorphic phantoms for use in dosimetry studies. J Appl Clin Med Phys 2009;10(3):2986.

187. Vose D. Risk Analysis: A Quantitative Guide. Third ed: Wiley; 2008.

188. Zaidi H, Ay MR. Current status and new horizons in Monte Carlo simulation of X-ray CT scanners. Med Biol Eng Comput 2007;45(9):809-17.

189. Caon M, Bibbo G, Pattison J. A comparison of radiation dose measured in CT dosimetry phantoms with calculations using EGS4 and voxel-based computational models. Phys Med Biol 1997;42(1):219-29.

190. Andreo P. Monte Carlo techniques in medical radiation physics. Phys Med Biol 1991;36(7):861-920.

191. Ay MR, Zaidi H. Development and validation of MCNP4C-based Monte Carlo simulator for fan- and cone-beam x-ray CT. Phys Med Biol 2005;50(20):4863-85.

192. Ludlow JB, Walker C. Assessment of phantom dosimetry and image quality of i-CAT FLX cone-beam computed tomography. Am J Orthod Dentofacial Orthop 2013;144(6):802-17.

193. Tapiovaara M, Sisskonen T. PCXMC: A Monte Carlo program for calculating patient doses in medical x-ray examinations. 2nd Ed ed. Helsinki, Finland: Radiation and Nuclear Safety Authority of Finland; 2008.

194. Cristy M. Mathematical phantoms representing children of various ages for use in estimates of internal dose. Oak Ridge, TN: Oak Ridge National Laboratory; 1980.

195. Cristy MEK. Specific absorbed fractions of energy at various ages from internal photon sources. Oak Ridge, TN: Oak Ridge National Laboratory; 1987.

196. Bakai A, Alber M, Nusslin F. A revision of the gamma-evaluation concept for the comparison of dose distributions. Phys Med Biol 2003;48(21):3543-53.

197. Smans K, Tapiovaara M, Cannie M, and co-workers. Calculation of organ doses in x-ray examinations of premature babies. Med Phys 2008;35(2):556-68.

198. Ludlow JB. Dose and risk in dental diagnostic imaging: with emphasis on dosimetry of CBCT. Korean J Oral Maxillofac Radiol 2009;39:175-84.

199. Kim DS, Rashsuren O, Kim EK. Conversion coefficients for the estimation of effective dose in cone-beam CT. Imaging Sci Dent 2014;44(1):21-9.

200. Schmidt PW, Dance DR, Skinner CL, Smith IA, McNeill JG. Conversion factors for the estimation of effective dose in paediatric cardiac angiography. Phys Med Biol 2000;45(10):3095-107.

201. Schlattl H, Zankl M, Petoussi-Henss N. Organ dose conversion coefficients for voxel models of the reference male and female from idealized photon exposures. Phys Med Biol 2007;52(8):2123-45.

202. Lamart S, Bouville A, Simon SL, and co-workers. Comparison of internal dosimetry factors for three classes of adult computational phantoms with emphasis on I-131 in the thyroid. Phys Med Biol 2011;56(22):7317-35.

203. Lee C, Lodwick D, Hasenauer D, and co-workers. Hybrid computational phantoms of the male and female newborn patient: NURBS-based whole-body models. Phys Med Biol 2007;52(12):3309-33.

204. Park S, Lee JK, Lee C, Lee C. Dosimetry calculations for internal electron sources using a Korean reference adult stylised phantom. Radiat Prot Dosimetry 2008;130(2):186-205.

205. Chao TC, Xu XG. Specific absorbed fractions from the image-based VIP-Man body model and EGS4-VLSI Monte Carlo code: internal electron emitters. Phys Med Biol 2001;46(4):901-27.

206. Pazik FD, Staton RJ, Williams JL, and co-workers. Organ and effective doses in newborns and infants undergoing voiding cystourethrograms (VCUG): a comparison of stylized and tomographic phantoms. Med Phys 2007;34(1):294-306.

207. Smith TJ, Phipps AW, Petoussi-Henss N, Zankl M. Impact on internal doses of photon SAFs derived with the GSF adult male voxel phantom. Health Phys 2001;80(5):477-85.

208. Helmrot E, Pettersson H, Sandborg M, Alten JN. Estimation of dose to the unborn child at diagnostic X-ray examinations based on data registered in RIS/PACS. Eur Radiol 2007;17(1):205-9.

209. Khelassi-Toutaoui N, Berkani Y, Tsapaki V, and co-workers. Experimental evaluation of PCXMC and prepare codes used in conventional radiology. Radiat Prot Dosimetry 2008;131(3):374-8.

210. Luckey TD. Radiation hormesis: the good, the bad, and the ugly. Dose Response 2006;4(3):169-90.

211. Luckey TD. Atomic bomb health benefits. Dose Response 2008;6(4):369-82.

212. Vaiserman A, Mekhova LV, Koshel NM, Voitenko VP. [Cancer incidence and mortality after low-dose radiation exposure: epidemiological aspects]. Radiats Biol Radioecol 2010;50(6):691-702.

213. Vaiserman AM. Radiation hormesis: historical perspective and implications for low-dose cancer risk assessment. Dose Response 2010;8(2):172-91.

214. Crump KS, Duport P, Jiang H, and co-workers. A meta-analysis of evidence for hormesis in animal radiation carcinogenesis, including a discussion of potential pitfalls in statistical analyses to detect hormesis. J Toxicol Environ Health B Crit Rev 2012;15(3):210-31.

215. Jolly D, Meyer J. A brief review of radiation hormesis. Australas Phys Eng Sci Med 2009;32(4):180-7.

216. AAPM. AAPM Position Statement on Radiation Risks from Medical Imaging Procedures, PP 25-A. College Park, MD: American Association of Physicists in Medicine; 2011.

217. Pearce MS, Salotti JA, Little MP, and co-workers. Radiation exposure from CT scans in childhood and subsequent risk of leukaemia and brain tumours: a retrospective cohort study. Lancet 2012;380(9840):499-505.

218. Mathews JD, Forsythe AV, Brady Z, and co-workers. Cancer risk in 680,000 people exposed to computed tomography scans in childhood or adolescence: data linkage study of 11 million Australians. Bmj 2013;346:f2360.

219. NCRP. Limitiation of Exposure to Ionizing Radiation, NCRP Report No. 116. Bethesda, MD: National Council on Radiation Protection and Measurements; 1993.

220. Qu XM, Li G, Ludlow JB, Zhang ZY, Ma XC. Effective radiation dose of ProMax 3D cone-beam computerized tomography scanner with different dental protocols. Oral Surg Oral Med Oral Pathol Oral Radiol Endod 2010;110(6):770-6.